An empirical study on the persuasive particle size effects over the multi-physical properties of monophase MWCNT-Al_2O_3 hybridized nanofluids

S. Suseel Jai Krishnan [a], M. Momin [a,b], C. Nwaokocha [a,c], M. Sharifpur [a,d,*], J.P. Meyer [a,e]

[a]Clean Energy Research Group, Department of Mechanical & Aeronautical Engineering, University of Pretoria, Pretoria 0002, South Africa
[b]Department of Mechanical Engineering, Kordofan University, Al Obied, Sudan
[c]Department of Mechanical Engineering, Olabisi Onabanjo University, Ago-Iwoye, Nigeria
[d]Department of Medical Research, China Medical University Hospital, China Medical University, Taichung 404, Taiwan
[e]Department of Mechanical and Mechatronics Engineering, Stellenbosch University, Matieland 7602, South Africa

*Corresponding author at: Clean Energy Research Group, Department of Mechanical & Aeronautical Engineering, University of Pretoria, Pretoria 0002, South Africa. E-mail address: mohsen.sharifpur@up.ac.za (M. Sharifpur)

Highlights

- Synthesizing MWCNT: Al_2O_3 at six different PWR each, with 5 nm and 30 nm Al_2O_3.
- Measuring the fluid properties to identify the best PWR based on the particle size.
- Maximum pH, electrical conductivity and viscosity with 30 nm Al_2O_3 at 10:90 PWR.
- Maximum pH, viscosity and thermal conductivity with 5 nm Al_2O_3 at 90:10 PWR.
- Property correlation predicted for different sized Al2O3 at all PWR of MWCNT: Al_2O_3.

Abstract

Hybrid nanofluids are colloidal suspensions containing two different nanoparticles whose enhanced thermal properties rely upon different parameters such as properties of the base fluid and nanoparticles, in addition to particle size and shape. While few studies have reported the best particle weight ratio (PWR) based on the optimal properties, no results have been found to declare the efficient PWR based on particle sizes. The current study focuses on measuring the fluid properties of hybrid (MWCNT-Al_2O_3) nanofluids with 5 nm and 30 nm Al_2O_3 at different temperatures (15 to 55 °C), particle concentrations (0.025 to 0.5%), and particle weight ratio (90:10, 80:20, 60:40, 40:60. 20:80, 10:90). When 0.1% volume concentrated nanofluids were compared based on particle size, the maximum enhancement for pH and electrical conductivity (σ) was 9.8 to 15.9% and 195.5 to 229.1% owing to the 80:20 ratio nanofluids with 5 nm Al_2O_3. In contrast, the viscosity and thermal conductivity enhancement were higher with 30 nm Al_2O_3 nanofluids by 17.5 to 21.7% for 10:90 ratio and 7.3 to 25.9% for 40:60 ratio. After measuring the properties of hybrid nanofluids with 5 nm Al_2O_3 at different PWR, temperature, and volume concentrations, the 90:10 ratio possessed the maximum enhancement in properties. The maximum pH, and σ enhancement were 14.5 to 23.3%, and 238.2 to 248.3% at 0.2% concentration, whereas viscosity and thermal conductivity enhanced by 40.9 to 57.3%, and 13.7 to 45.1% at 0.5%

concentration. Correlations were computed to predict relative values that have R-square values between 0.9160 and 0.9926, with a margin of deviation away from experimental values by −9.42 and + 6.83%.

Keywords: Hybrid nanofluids; Percent weight ratios; Al_2O_3; MWCNT; pH; Viscosity; Thermal conductivity; Electrical Conductivity; Stability; Particle size; Interaction mechanism

Nomenclature

Ag	Silver
AlN	Aluminium nitride
Al_2O_3	Aluminium oxide
Au	Gold
BF	Base fluid
BG	Bio-glycol
BNF	Binary nanofluid
BNP	Binary nanoparticle
CNT	Carbon nanotube
Cu	Copper
CuO	Copper oxide
DIW	Deionised water
DW	Distilled water
DWCNT	Double-walled carbon nanotube
EG	Ethylene glycol
EG-DIW	Ethylene Glycol-deionised water
EO	Engine oil
Fe_2O_3	Iron (III) oxide
Fe_3O_4	Iron (II) oxide
G	Graphene
GA	Gum Arabic
GO	Graphene oxide
k	Thermal conductivity, W/m K
LaB_6	Lanthanum hexaboride
MgO	Magnesium oxide
MO	Mineral oil
MWCNT	Multi-walled carbon nanotube
ND	Nano-diamond
NF	Nanofluid
NP	Nanoparticles
PVP	Polyvinyl pyrrolidone
PWR	Particle Weight Ratio
SDS	Sodium dodecyl sulphate
PG	Propylene glycol
SDBS	Sodium dodecyl benzene sulfonate
SiC	Silicon carbide
SiO_2	Silicon oxide
SWCNT	Single-walled carbon nanotube
T	Temperature, °C
TiO_2	Titanium oxide
TO	Transformer oil
V	Volume, m^3
w	weight, g
ZnO	Zinc oxide

Greek letters

γ	Gamma phase of Aluminium oxide
ρ	Density, m^3/kg
μ	Dynamic viscosity, Pa.s
σ	Electrical conductivity, S/cm
φ	Volume fraction
ϕ	Volume concentration, vol.%

Subscripts

av	Average
bf	Base fluid
Exp	Experiment
Enhan.	Enhancement
hnf	Hybrid nanofluid
Pred	Predicted
rel	Relative
s	Sample
w	Water

1. Introduction

Nanofluids' (NFs) continuous exhibition of exceptional flow and thermal behavior compared to conventional heat transfer fluid makes a subject of increasing global research [1], [2], [3]. Studies on the thermal properties of NFs show enhancement compared to base fluids (BFs) [4], [5], [6]. Various nanoparticles (Ag, AIN, Al_2O_3, Au, Cu, CNT, CuO, DWCNT, Fe_2O_3, Fe_3O_4, G, MgO, MWCNT, ND, SiC, SiO_2, spinels, SWCNT, TiO_2, ZnO, etc.) dispersed in various BFs (W, BG, coconut oil, EG, EO, PG, MO, TO, palm oil, glycerol, ionic fluid, etc.) at varying mass/weight/volume fractions or concentration for ranges of temperatures, were studied [7], [8], [9]. Dispersants or surfactants (DATB, GA, Oleic acid, PVP, Salt, SDBS, SDS) make the nanofluids stable by reducing the surface energy of host fluids, thus increasing the dispersibility of nanoparticles [10], [11], [12]. Binary nanofluids (BNFs) are doing well in improving thermal applications because of their appreciable thermophysical properties over base fluid [13]. It gives good credence to tri-hybrid nanofluids (TNFs). These nanomaterials blend their combined physical and chemical properties. This growth has positively impacted nanofluids research, leading to the hybridization of different nanoparticles with various nanosize, nanoshape, temperatures, and base fluid to formulate hybrid and tri-hybrid nanofluids. The use of mono, di- and tri-hybrid nanofluids as novel working fluids has gained

global attention and widespread application spanning nano-lubrication [14], [15], [16], corrosion control [17], and electronic cooling applications [18], [19], solar thermal applications [20], [21], [22].

Over a decade now, the concept of hybridizing NPs was first advanced by Jana et al. [23] and Chopkar et al. [24], who were the ones to come up with the concept of hybridizing different nanomaterials for optimized thermal solutions. These works reported improved thermal conductivity (k). They published a k improvement of 50–150% when they synthesized Ag_2Al and Al_2Cu BNPs in EG and water to formulate BNFs for volume concentration (ϕ) range of 0.20 to 1.50 vol%. Contrariwise, Jana *et al.* [23] formulated and measured *k* for water-based single-NFs (Au, CNT, and Cu) and water-based BNFs (CNT-Au and CNT-Cu). They reported that the single-NFs had a higher *k* than the BNFs. Jha et al. [25] published k of Cu-MWCNT dispersed in DIW and EG had a higher value than that of NFs of MWCNT/EG and MWCNT/DIW, which supported the finding of Chopkar et al. [24] and in agreement with the results of Chen et al. [26], who reported an improved k of Ag–MWCNT/Water BNF over the MWCNT/water NF.

Using Fe_3O_4–GNP (20:80)/DIW NF, Askari et al. [27] considered the impact of temperature (20–40 °C) and a mass fraction (0.1–1.0 mass%) on thermal conductivity (*k*) and observed 14–32% improvement. Chen et al. [26] examined *k* for MWCNT (0.05 vol%)–Fe_2O_3 (0.02 vol%) aqueous-based NF at room temperature. They published a 27.75% improvement over the BF. Also, Esfahani et al. [28] published an enhanced thermal conductivity for ZnO–Ag/W nanofluid, as φ (0.125–2%) and temp. (25–60 °C) increases. Under the impact of φ (0.10–3.50%) and temperature (25 to 50 °C), Toghraie et al.[29] Investigated k of ZnO-TiO_2/EG BNF and reported an improved k under growing volume fraction and temperature. At 3.5 vol% and 50 °C, the maximum k enhancement of 32% was achieved. In addition, Chen et al. [26] published the *k* of aqueous-based Ag–MWCNT BNF to be more than *k* of aqueous-based MWCNT/W NF for 1.0% volume fraction and temperature 5–65 °C. Suresh et al. [30] experimentally studied the viscous behavior and thermal conductivity $0.9Al_2O_3$-0.1Cu/water BNF at ambient temperature for volume concentrations (0.1–2%). The authors observed thermal conductivity and viscosity enhancement of BF by 1.47–12.11% and 8–115%, respectively. Recently, Rostami et al. [31] studied the *k* for GO-CuO(50–50)/W-EG (50:50) nanohybrid at increasing φ of 0.1 to 1.60 vol% for temperatures 25 to 50 °C. They obtained the highest enhancement of 43.4% when φ was 1.6 vol% at 50 °C. Lately, the influence of variation in φ (0.005–0.1 vol%), temperatures (25–40 °C), and PMRs (30:70, 50:50, 70:30) on the *k* of Al_2O_3-Ag/DW BNF was examined by Aparna et al. [32]. The authors published the highest *k* with the 50:50 ratio. The BNF had a maximum *k* than the NFs of Ag/DW and Al_2O_3/DW. The enhancement increased with increasing volume concentration.

For heat transfer applications using nanohybrids, viscosity (μ) is a prime parameter. Soltani and Akbari [33] examined the influence of temperature range 30 to 60 °C and particle concentration 0 to 1.0% on μ of MgO-MWCNT/EG BNF and observed a Newtonian performance with μ in a detracting trend at temperature increase and enriched μ at increased particle concentration. Next, Asadi and Asadi [34] examined the μ of MWCNT-ZnO/Engine Oil (10 W40) BNF and reported temperature having a higher impact on μ than particle concentration, thus achieving a maximum deterioration in dynamic viscosity of 85% for temperature 55 °C. Also, Motahari et al. [35] examined the μ of MWCNT-SiO_2/SAE20W50

BNF at ϕ = 0.05–1.0 vol% and temperature of 40 to 100 °C. The nanohybrid exhibited Newtonian behavior for all concentrations and temperatures, with an enhanced μ of 171% at peak particle concentration and temperature.

Open literature is available for the measurement of k and μ of nanosuspensions. Esfe et al. [36] evaluated the k and μ of an aqueous-based nanohybrid of Ag–MgO (50:50) for φ = 0–2% and achieved augmentation with increasing φ. Considering changes in temperatures (30–60 °C), PMRs (25:50, 50:50, and 75:25), and φ (0.1–0.5 vol%), Mechiri et al. [37] evaluated experimentally for μ and k of Cu–Zn (50:50)/groundnut HNF. They noticed that φ and temperature affect μ and k more than PMR. Both BF and nanohybrid exhibited Newtonian behavior. Suresh et al. [30] reported an enhancement of 8–115% for μ and 1.47–12.11% for k for an aqueous-based Cu-Al_2O_3 (10%:90%) BNF at φ = 0.1–2%. Also, Hamid et al. [38] studied k and μ for TiO_2–SiO_2 (40–60)/W-EG (60:40) BNF for changing PMRs (20:80–80:20) for temperatures 30–80 °C at φ = 1.0 vol%. They reported an enhancement of 16% for k at PMR 20:80 and maximum improvement for μ for PMR 40:60, assuring it is suitable for thermal cooling purposes. PMR of 50:50 has the poorest cooling properties.

Investigating the electrical conductivity (σ) of water-based Al_2O_3–TiO_2 and Al_2O_3–SiO_2 BNFs for temperature (20–60 °C) and φ (0.5:0.5, 0.5:1.0, 0.5:1.5 (for both Al_2O_3:TiO_2 and Al_2O_3:SiO_2)), Chereches and Minea [39] published a σ enhancement of 30–58-fold and 14–40-fold for TiO_2/water and SiO_2/water NFs, respectively, when compared to BF at 60 °C and φ (0.5:1.5). The σ of TiO_2/water NFs is more than SiO_2/water NFs. Hence highest σ of Al_2O_3–TiO_2/Water BNF was 43–57-fold as related to water. Also, Giwa et al. [40] investigated the influence of PMRs (20:80, 40:60, 60:40, 80:20, and 90:10) and temperatures 15–55 °C on the σ and μ of Al_2O_3–MWCNT/DIW BNF. They obtained a peak augmentation of 288.0% and 19.3%, and 442.9% and 26.3% for μ and σ of Al_2O_3–MWCNT/DIW BNF at PMRs of 20:80 and 90:10, respectively, compared to BF. Also noticed is that with growing temperatures, μ detracts clearly, while PMR considerably enhanced σ, which classifies as fine for coolant applications. Again, Giwa et al. [41] first investigated the trio effect of temperature (20–50 °C), φ (0.05–0.75 vol%), and BFs (EG-DIW and DIW) on the performance of μ and σ of nanohybrid of Al_2O_3– Fe_3O_4 (25:75). Authors published augmentation for σ of 163.37–1692.16% and 717.14–7618.89%, whereas μ was improved by 3.23–43.64% and 2.79–49.38% for the DIW-based and EG–DIW-based nanohybrid, in comparison to the individual BF. Further discovery reveals that enhancing φ enhances σ and μ, while an increasing temperature enhances σ and detracts μ. The DIW-based BNF possessed minimal μ and maximum σ over the EG–DIW-based nanohybrid. Lately, Wanatasanapan et al. [42] considered the impact of Al_2O_3-TiO_2 NPs mixing composition on the thermal-fluid behavior of the water-based BNFs. The water-based BNFs were formulated with five various ratios of Al_2O_3 and TiO_2 NPs at a constant 1.0 vol% for temperatures 30–70 °C. They reported a maximum k of 1.134 W/mK for a sample ratio of 50:50 at 70 °C, with a k enhancement of 71% compared with DIW. The BNFs exhibited a Newtonian fluid pattern for all NPs temperature and mixing ratios, with the ratio of 80:20 having the maximum μ of 1.98 mPas. Furthermore, Giwa et al. [43] investigated the trio impact of PWRs (20:80, 40:60, 60:40, 80:20), NS, and temperature (20–50 °C) on the thermal performance of MgO (20 and 100 nm)-ZnO/DIW BNF at 0.1 vol%. They reported that BNF with 100 nm MgO NP had higher values of σ, μ, and pH than BNF with 20 nm MgO NP, except for k. Also, temperature increase enhances k and σ of the nanohybrids but detracts μ and pH. Maximum

improvement for k, μ, and σ are 14.95–22.33% (40:60), 8.29–17.46% (60:40) and 453.70–550.62% (40:60), respectively.

Akilu et al. [44] performed an investigation on c_p, k, and μ of SiO_2–CuO/C (80:20)/EG-G (40:60) BNF by changing φ (0.5–2.0 vol%) and temperature (30–80 °C). They observed enhancement of 26.9% and 1.15-fold for k and μ, respectively, while c_p deteriorated by 21.10% at φ of 2.0 vol%, at 80 °C. The k for BNF is more improved than the k (6.9%) of SiO_2/G-EG. Further, Kannaiyan et al. [45] studied the ρ, c_p, k, and μ of Al_2O_3–CuO/EG-W (80:20) BNF for temperature (20–70 °C) and volume concentration (0.05, 0.1, and 0.20 vol%). They reported an improvement of thermal properties with augmentation in φ, k increased with temperature, ρ and μ reduced steadily with temperature increase, while c_p remained constant. The maximum achieved k improvement was 45%.

Studies keep emerging on the use of nanofluids for thermal management applications. However, from open literature, we lack an investigation that aims at predicting the optimal PWR based on the particle size. Therefore, industries and commercial sectors would be misguided to synthesize the hybrid nanofluids based on the reported PWR as the overall properties appear to vary based on the particle size and shape. Hence, to fill the existing research gap, there must be a mapping of the 4th parameter, namely the particle size with the pre-existing trio parameters such as percent weight ratios (PWRs), temperature, and concentration (ϕ) on different properties of nanohybrids such as pH, electrical conductivity, density, specific heat, viscosity, and thermal conductivity. Besides, the best nanoparticles available to date (MWCNT and Al_2O_3) are the considerations for this study. Moreover, this is the first time the nanofluid properties attain importance for measurement after confirming 4-month stability.

2. Experimental details

2.1. Raw sources for sample synthesis

Nanoparticles of γ-Al_2O_3 with two different particle sizes sourced from Nanostructured and Amorphous Materials Inc., USA and functionalized MWCNT with COOH content of 1.45 to 1.65 obtained from MKNano Company, Ontario, Canada, were utilized in this study. In addition, SDS (Sodium dodecyl sulfate) per purity of ≥ 98.5% sourced from Germany, Sigma-Aldrich, was engaged as a dispersant/surfactant to achieve superior hybrid nanofluids stability. The properties of these nanopowders are listed in Table 1.

Table 1. Properties of the nanopowders.

Properties	Al_2O_3		COOH-CNT
Particle size	30 nm	5 nm	Length 10–30 μm; ID: 3–5 nm; OD: 10–20 nm
Purity	~99%	~98%	~97%
Colour	White	White	Black
Shape	Spherical	Spherical	Tubular
Density (g/cc)	3.97	3.88	2.2
Specific heat (J/kg K)	878	882	717
Specific Surface Area (m^2/g)	182	540	237
Thermal conductivity (W/mK)	40	42	3000

2.2. Instrumentation capabilities

PANalytical X'Pert Pro X-Ray Powder Diffractometer (XRD), Zeiss Crossbeam 540 Scanning Electron Microscopy (SEM), JEOL JEM-2100F Transmission Electron Microscope (TEM), were engaged for powder and fluid characterization in this study. The particle's hydrodynamic size and the zeta potential were measured by Malvern Zetasizer Nano ZS ZEN 3600 instrument. Suitably using a digital weighing machine (accuracy of ± 0.01 g and measurement variety of 10 mg – 220 g - Radwag AS 220.R2 (Poland)), the powders were weighed based on the volume concentrations prescribed for the study. A magnetic stirrer (Hotplate Stirrers, Ha400 HSB, Indonesia) and Qsonica device (ultrasonicator- Model Q-700; 700 W and 20 kHz USA) was engaged to homogenize the hybrid nanoparticles into the deionized water and to mix the powder MWCNT and γ-Al_2O_3 nanoparticles, respectively. The stability of the nanofluids was also quantified using UV Vis Spectrophotometer (Jenway, UK). The mixture temperature during the sonication period was kept constant at 20 °C by inserting the samples into a programmable thermal bath (LAUDA ECO RE1225). EUTECH (CON700) electrical conductivity meter (±1% accuracy), Jenway 3510 pH meter (±0.003 accuracy and 2 to 19.999 range), KD2 Pro thermal conductivity meter (Decagon devices, US; ± 10%% accuracy for k = 0.2 – 2.0 W/m K), SV-10 device (sine wave viscometer with ± 3% accuracy, A&D, Japan) to measure the thermal, electro, and chemico-physical properties of the prepared nanofluid samples, were used.

2.3. Formulation of hybridized nanofluid

A two-step method to make water-based (γ-Al_2O_3/MWCNT) hybrid nanofluids was engaged. Eq.(1) calculates the weight of the nanoparticles required. Thus, the specific amount of oxide nanoparticles and nanotubes was formulated at 0.1 vol% for dispersion into the based fluid. In the next step, the powder Al_2O_3 nanoparticles and MWCNT nanotubes have been dispersed at the ratio of 40:60 by weight into water base fluid using a magnetic stirrer for 30 min with a magnetic agitator. The process of stirring followed by a sonication procedure using an ultrasonic device is the usual preparation method. The idea behind using an ultrasonic processor is to attain an excellent distribution and eliminate the phenomenon of nanoparticle clustering, thus, preventing the issue of sedimentation and making a stable suspension of nanofluids. The fluid sample was susceptible to different sonication periods (30–90 min), amplitude (70–90), and dispersion fraction of surfactant (0.4–1.4) to optimize the stable preparation of the remaining nanofluid samples. To confirm worthy stability, pH

and Electrical Conductivity of the prepared hybrid nanofluids at different PWR (MWCNT/Al_2O_3-90:10, 80:20, 60:40, 40:60, 20:80, and 10:90) for 0.025, 0.05, 0.1, and 0.2% were studied. The crystallite size, powder morphology, and particle dispersion in the HNFs via XRD, SEM, and TEM, were respectfully measured. The stability of the fluids was also inferred through viscous behavioral measurements at room temperature for four months, and visual techniques to observe the stability of the HNFs were engaged. Based on the same procedure by Giwa et al. [40], once again, the fluids for testing and comparison were also formulated.

$$\phi = \frac{\left[\left(\frac{w}{\rho}\right)_{MWCNT} + \left(\frac{w}{\rho}\right)_{Al_2O_3}\right] \times 100}{\left(\frac{w}{\rho}\right)_{MWCNT} + \left(\frac{w}{\rho}\right)_{Al_2O_3} + \left(\frac{w}{\rho}\right)_{base\ \ fluid}} \quad (1)$$

2.4. Quantifying the thermo, electro and chemico-physical properties

2.4.1. Thermal conductivity of HNFs

The quantification of the functional requisite by the fluid to conduct heat was through the KD2 Pro meter. The container with nanofluid was positioned in the thermal bath to maintain the measurement's temperature constant at different ranges (15 to 60 °C). Meanwhile, the device calibration was made by measuring the thermal conductivity of the standard fluid provided by the manufacturer (glycerin). To assure the accuracy of the experimental data, the measurement was recurrent eight times at each temperature, and the average value resulted in the investigational data. Equations (2), (3) calculated the thermal conductivity of all the samples, relative and enhancements concerning the base fluid.

$$\mathrm{k_{rel}} = \frac{\mathrm{k_{hnf}}}{\mathrm{k_{bf}}} \quad (2)$$

$$\mathrm{k_{enhan.}}(\%) = \left(\frac{\mathrm{k_{hnf}} - \mathrm{k_{bf}}}{\mathrm{k_{bf}}}\right) \times 100 \quad (3)$$

Where $\mathrm{k_{rel}}, \mathrm{k_{hnf,}}\ \mathrm{k_{bf}}\ \ \mathrm{and}\ \mathrm{k_{enhan}}$ are the relative thermal conductivity, the thermal conductivity of HNFs, based fluid thermal conductivity, and the thermal conductivity enhancement. Also, the margin of deviation (MOD) for thermal properties of the considered binary nanofluid is evaluated based on Equation (4).

$$\mathrm{MOD}(\%) = \left(\frac{\mathrm{M_{Exp}} - \mathrm{M_{Pred}}}{\mathrm{M_{Exp}}}\right) \times 100 \quad (4)$$

where M_{Pred} and M_{Exp} are the forecast and investigational values of a point out property, respectively.

The uncertainty of k was evaluated using Equation (5), within the 95% probability. From the means of repeatability, reproducibility, manufacturer's data, and the temperature indication, the measure of uncertainty was calculated and found to be 2.18%.

$$U_k = \sqrt{\left(\frac{\Delta m}{m}\right)^2 + \left(\frac{\Delta V}{V}\right)^2 + \left(\frac{\Delta T}{T}\right)^2 + \left(\frac{\Delta k}{k}\right)^2} \quad (5)$$

2.4.2. Evaluating the fluid viscous behavior

Before measuring the viscous behavior of the base fluids at 15–60 °C temperature, the SV-10 device was calibrated. During the evaluation, the temperature was controlled using a circulating water bath (LAUDA ECO RE1225) after adjustment with the base fluids. Relative viscosity and enhancement of the HNFs related to base fluids were estimated by Eqs. (4), (5), respectively.

$$\mu_{rel} = \frac{\mu_{hnf}}{\mu_{bf}} \quad (6)$$

$$\mu_{enhan.}(\%) = \left(\frac{\mu_{hnf} - \mu_{bf}}{\mu_{bf}}\right) \times 100 \quad (7)$$

Where μ_{hnf}, and μ_{bf} are the viscosity of HNFs and the DIW, respectively.

In addition, the margin of deviation (MOD) for both characteristics of the HNFs examined is stated by Equation (8).

$$\mathbf{MOD}(\%) = \left(\frac{\mathbf{V_{Exp.}} - \mathbf{V_{Pred.}}}{\mathbf{V_{Exp.}}}\right) \times 100\% \quad (8)$$

Where $V_{Exp.}$ and $V_{Pred.}$ are experimental and predicted values of the specific property.

The uncertainty of the μ was evaluated using Equation (9), within the 95% probability. Based on the calibrated data, repeatability, temperature indication, and manufacturer specification, the uncertainty was 1.26%.

$$U_\mu = \sqrt{\left(\frac{\Delta m}{m}\right)^2 + \left(\frac{\Delta V}{V}\right)^2 + \left(\frac{\Delta T}{T}\right)^2 + \left(\frac{\Delta \mu}{\mu}\right)^2} \quad (9)$$

2.4.3. Measurement of electrical conductivity and pH of formulated nanofluid

Calibration of the EUTECH instrument using a standard fluid (as supplied by the maker) ensures proper electrical conductivity measurements. Proceeding with standardization, a worth of 1413 μS cm^{-1} was measured at 25 °C. After which, the electrical conductivity of deionized water base fluid and hybrid nanofluids at 15–60 °C (5 °C intervals) were measured. Before measuring the pH of the HNFs, calibration of the pH meter using fluid supplied (pH values of 10, 7, and 4) was carried. The relative (σ_{rel}) and the enhancement (σ_{enhan}) of the electrical conductivity regarding base fluids were calculated by Equations (6), (7), respectively. With the error propagating from the electronic weighing balance while measuring the surfactant and the nanopowders and the sensitivity of the pH meter based on the temperature indicated and repeatability of data, the uncertainty seemed to be

2.71%. Similarly, uncertainty based on the measured electrical conductivity values was 1.13%.

$$\sigma_{rel} = \frac{\sigma_{hnf}}{\sigma_{bf}} \tag{10}$$

$$\sigma_{enhan.}(\%) = \left(\frac{\sigma_{hnf} - \sigma_{bf}}{\sigma_{bf}}\right) \times 100 \tag{11}$$

Where σ_{hnf}, and σ_{bf} are electrical conductivity of hybrid nanofluids and the base fluid, respectively.

3. Results and discussion

3.1. Characterization of hybrid nanopowders nanofluids

3.1.1. Quantifying grain size and structure

The instrument used in this investigation is a PANalytical X'Pert Pro X-Ray Powder Diffractometer. The samples analyzed exhibit considerable peak broadening, and the counts are low (low intensities), signifying a small crystallite size. Before measuring, the crystallite size, the LaB_6 sample, a size-strain standard that indicates negligible size-strain broadening, was used. Its measurement was done on the same instrument using the same settings used later to measure the hybridized samples.

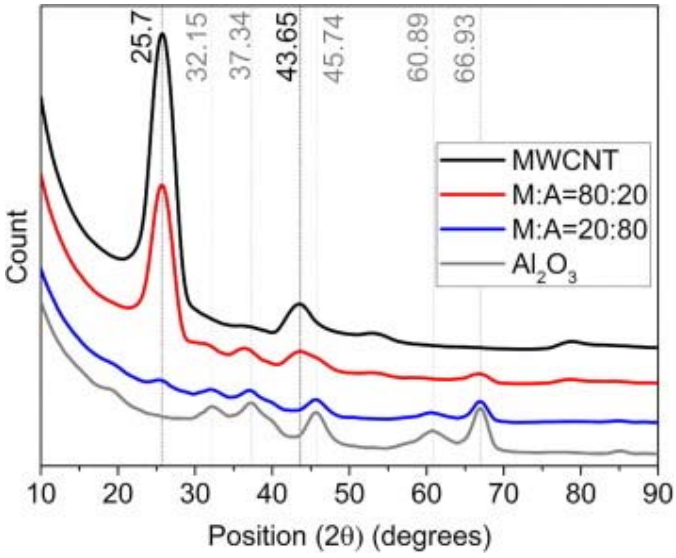

Fig. 1. X-ray diffraction spectra of mono and hybrid nanopowders.

Based on the obtained data, the XRD plots in Fig. 1 show multiple peaks for Al_2O_3 (5 nm) and MWCNT that matches well with the available literature works. The peaks corresponding to 25.70° and 43.65° correspond to MWCNT, and the ones prevailing at 32.15°, 37.34°, 45.74°, 60.89°, and 66.93° correspond to those of Al_2O_3. The hybrid powders of 80:20 and 20:80 ratio of MWCNT: Al_2O_3 clearly show the combined peaks of both powders. Based on the

Debye-Scherrer relation, the average crystallite sizes of MWCNT, Al_2O_3, and 80:20 ratio of MWCNT: Al_2O_3 and 20:80 ratio of MWCNT: Al_2O_3 was 2.38 nm, 2.49 nm, 3.39 nm, and 3.53 nm.

3.1.2. Morphological studies

We observed the morphology of the hybridized powder with the aid of Scanning Electron Microscopy. As notable from Fig. 2, the Al_2O_3 particles could be seen annexed towards the wall of the CNTs besides getting clustered within themselves. Besides, we observed that their sizes are more or less similar, as observable from how the periphery of Al_2O_3 matches that of MWCNT. We can infer the same from the crystallite sizes deduced from the XRD data. The spherical alumina associated with the walls partially supports the effect of enhanced electro- and thermo-phoretic behavior within the fluids when susceptible to electrical and thermal inertia.

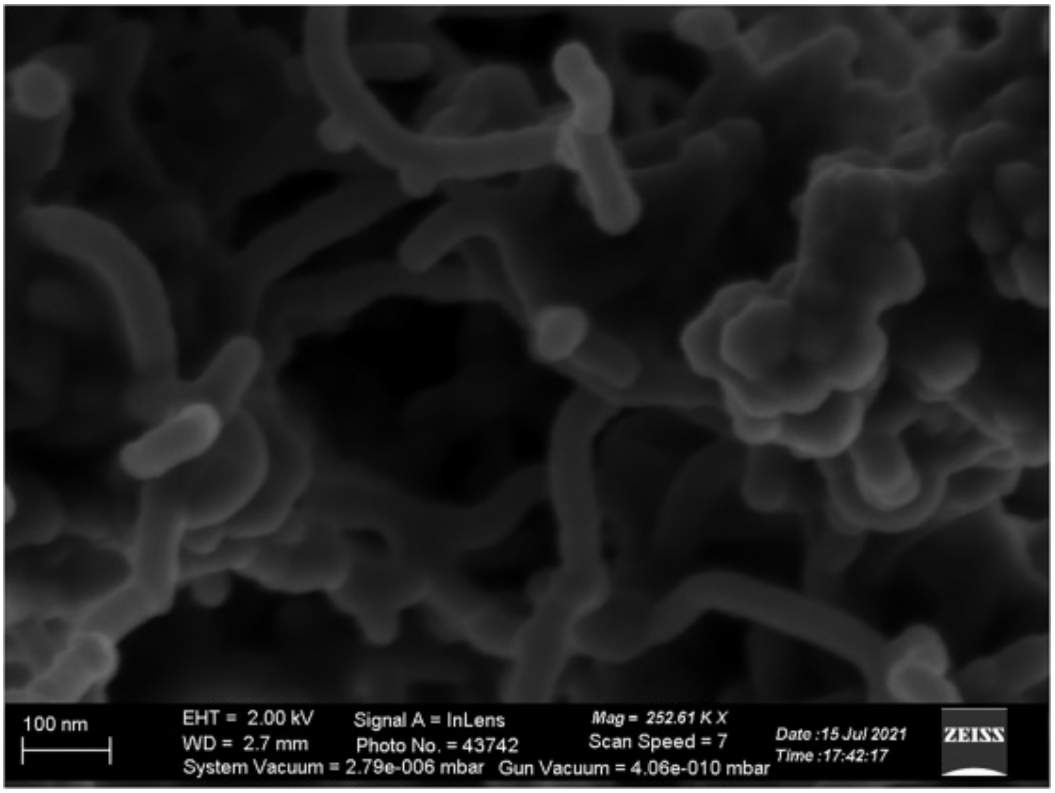

Fig. 2. Scanning Electron Micrograph of hybridized nanopowders.

3.2. Hydrodynamic size of the powder

The hydrodynamic diameter of the dispersed particle within a base fluid helps us understand the particle-to-fluid interaction. The hydrodynamic size of the powder sample measured by the Dynamic Light Scattering method (DLS) explains the overall diameter of the powder sample by taking into consideration the encapsulation of a thin electric dipole layer of the base fluid around the particle surface. This additional layer impacts the solid constituents within the base fluid. Thus we will also realize the particle motion by the

Brownian mechanism. In general, calculating the hydrodynamic diameter of the particle is through the translational diffusion coefficient from the Stokes-Einstein equation [46]. The TEM helps us identify the core size with a fluid layer around it. Thus, a more accurate measurement could be possible by DLS studies, and Fig. 3 shows the hydrodynamic size of 0.1% concentrated nanofluid prepared with PWR of 90:10 as 39 nm, which is 5 to 6 times more than the crystallite size measured by XRD, and particle size as specified by the manufacturer. As the particle diameter is relatively smaller, the Brownian motion must be higher, thus ensuring enhanced properties of the nanofluids.

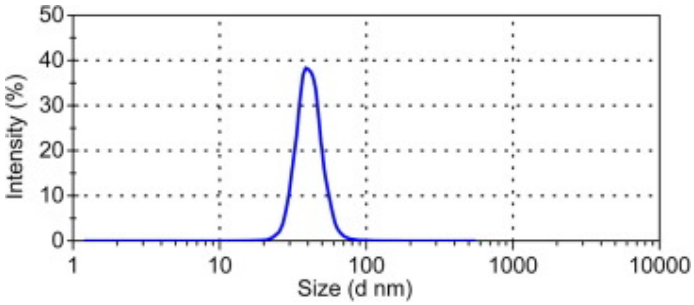

Fig. 3. Hydrodynamic size of 0.1% concentrated 90:10 nanofluid at pH = 8.8.

3.3. Optimized preparatory conditions for nanofluid synthesis

It is always a good practice to optimize the parameters desired for synthesizing, surfactant dispersion, sonicating, and stabilizing the nanofluids for the long run. Hence the charge bearing capacity of the powders dispersed into the base fluid is determined through electrical conductivity studies at different dispersion fractions (0.4 to 1.4), the amplitude of sonicating waves (70 to 90), and sonicating time (30 to 90 min). In general, the surfactant micelles that contain hydrophilic and hydrophobic regions encapsulate the powder particles. Once the surfactant concentration is sufficient to attach to the particle surfaces, the excess surfactant adheres to each other to form micelle clusters. The electrical conductivity would rise until a limit reaches, followed by a fall, which indicates the critical micelle concentration (CMC).

We noted that the electrical conductivity rose during the following conditions: dispersion fraction between 0.4 and 0.8, sonication amplitude at 70 and 75, and the sonicating time between 30 and 50 min. But the values suddenly declined at 1.0, 80, and 60 min, respectively, which are identified as optimized fluid preparatory parameters as notable from Fig. 4, after which the electrical conductivity values began to increase with a rise in such parameters.

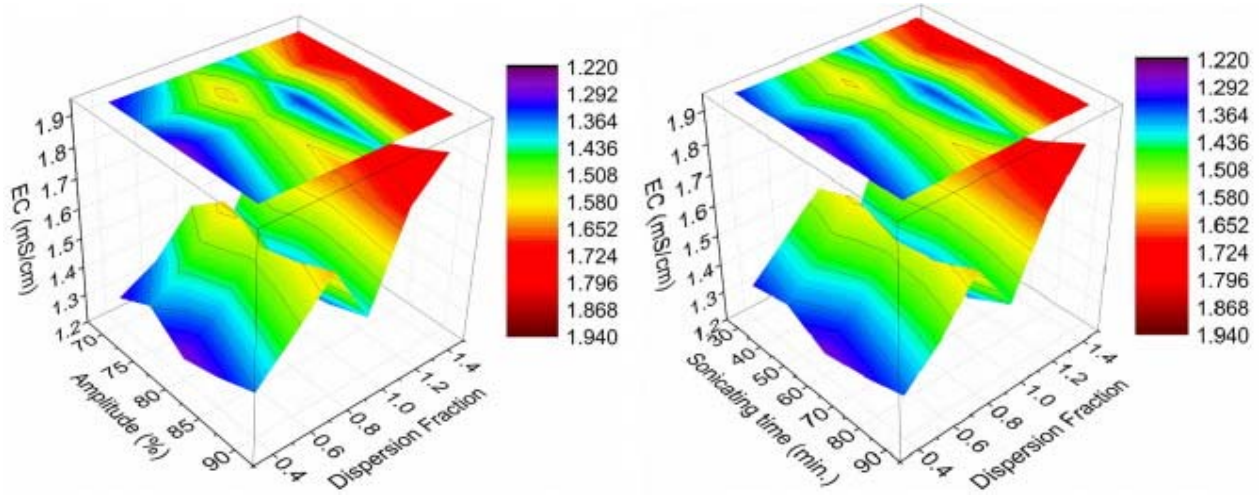

Fig. 4. Identifying optimised sonication time, sonicator amplitude and dispersion fraction with φ = 0.1% 60:40 MWCNT:Al_2O_3 nanofluid.

3.4. Characterization of hybridized nanofluids

The TEM image in Fig. 5 depicts the distribution of the hybridized particles within the aqueous base fluid. In general, MWCNTs are hydrophobic, and they must be dispersed and stabilized with surfactants, especially with aromatic groups in them, such as Sodium dodecylbenzene sulphonate and Triton X-100. However, such aromatic groups tend to enhance the viscous behavior that might look excellent for stabilizing but affects the thermo-convective behavior of these fluids. In our case, functionalized MWCNT were used, and they were stable only for 19 days. Our focus on the experiments were after attaining the stability for four months, and hence sodium dodecyl sulphate (SDS) was preferred. It is evident from the TEM image that the hybrid particles are nearly distributed. In addition, we found from the TEM image that the particle sizes were 11 nm in the case of MWCNT and 14 nm in the case of Al_2O_3, which is indicative of the hydrodynamic bonding of the powders with the associated fluid.

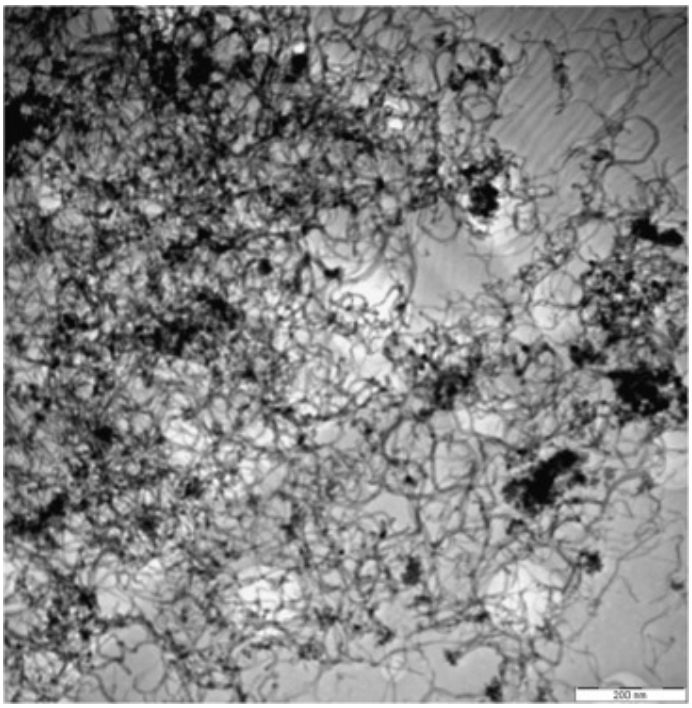

Fig. 5. Powder dispersion evaluations through Transmission electron microscopy.

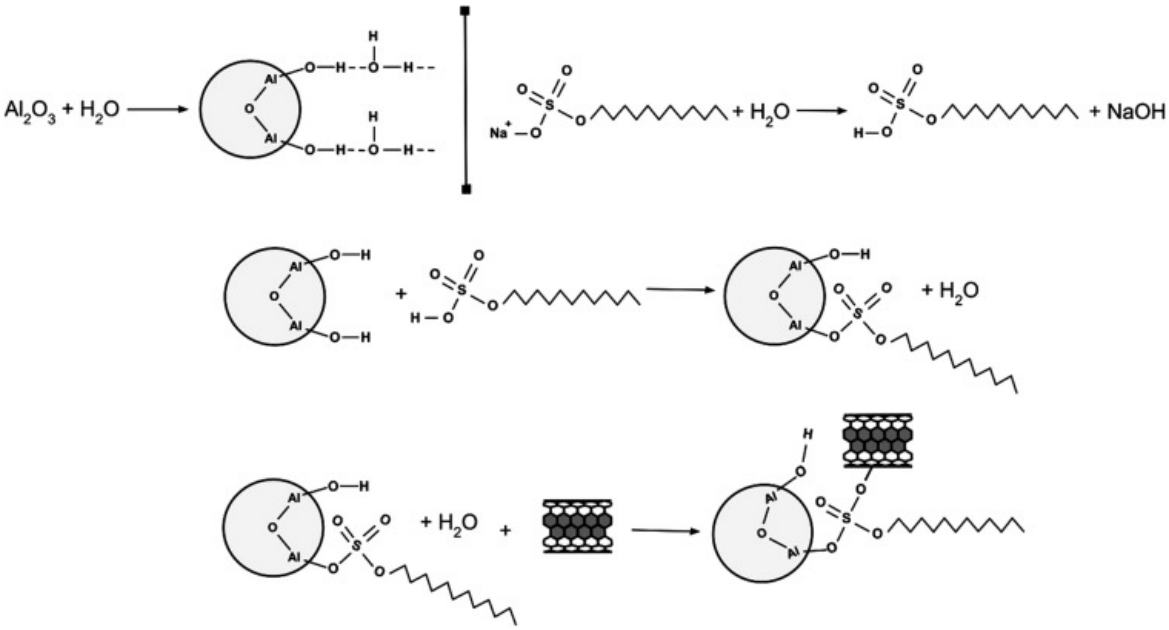

Fig. 6. Mechanism of particle interaction with surfactant and base fluid.

The possible mechanism for such stability or distribution is explanatory in Fig. 6. While aluminum oxide reacts readily with water, SDS mixes with water, thus releasing the sodium ion to form sodium hydroxide. The head of the surfactant thereon interacts with aluminum oxide nanofluid to discharge water molecules. While on the other end, the double bond of the oxygen in the surfactant molecule breaks to form a bond with the carbon atom available on the outer periphery of the MWCNT. Thus, they get acquainted with each other for a

much-stabilized solution. It is one of the reasons why Al_2O_3 is found abundant at sites where there is a long or series of MWCNTs.

3.5. Fluid stability quantification

3.5.1. Transient viscosity method

One of the promising methods to quantify the stability of the nanofluids is by measuring the viscous behavior of the nanofluids. We measured the viscosities of the 0.1% concentrated nanofluids at a 90:10 ratio of MWCNT: Al_2O_3 at regular intervals during and for a month (30 days) at an ambient temperature of 20 °C (refer to Fig. 7). The viscosities were also measured thrice every day to determine the average viscosity of the fluid for the day. Thus a total of 90 data were recorded. The viscous nature deteriorated merely by 2.03% over a period of 30 days is generally considered appreciable of the fact that the fluid remained stable for a prolonged period.

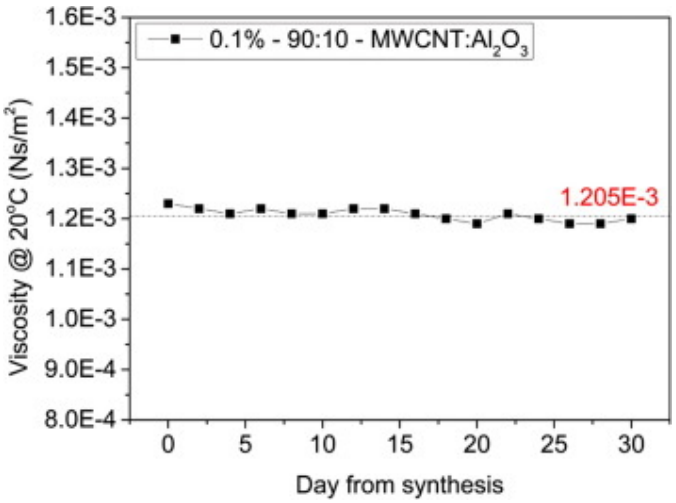

Fig. 7. Investigating the stability through viscosity measurement over a month.

3.5.2. Zeta potential measurement

Based on the existing research studies on the characterization of nanofluids, zeta potential stands unique in the method to evaluate the stability of nanofluids. The potential difference between the particle surface and the bulk fluid is zeta potential. The fluid stability is based on high electrostatic repulsion between the dispersed particles within the fluid, thus preventing them from being agglomerated. When the zeta potential is beyond ± 30 mV, it is considered a better stable fluid. The zeta potential appears to be excellent if the pH values indicate acidity or basicity, where the former links to more H^+ ions and the latter links to more OH^- ions, thus developing sufficient repulsive forces for the fluid samples to prevail stable.

Fig. 8 shows the zeta potential generated around the particles dispersed in 90:10 PWR at 0.1% concentration within the base fluid and maintained at pH = 8.8. The zeta potential of

−35 mV indicates a highly stable sample. If the pH could have been 10, the zeta potential would have been approximately −45 mV.

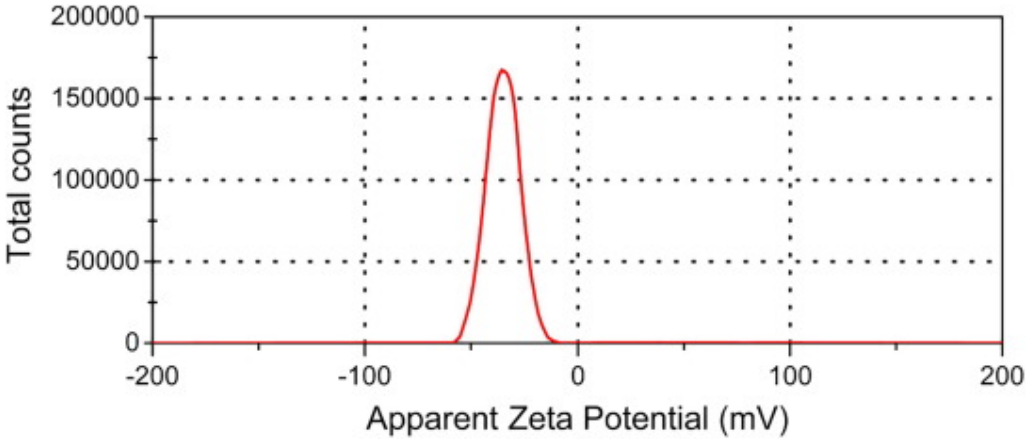

Fig. 8. Zeta potential measurement of 0.1% concentrated 90:10 nanofluid at pH = 8.8.

3.5.3. UV absorbance method

Performing the stability evaluation by UV Vis spectrophotometer for 40 h with an average interval of 20 min was based on two cases: (i) by comparing two best performing nanofluids, i.e., 90:10 MWCNT: Al_2O_3 containing 5 nm-sized Al_2O_3 and 40:60 PWR containing 30 nm Al_2O_3, (ii) by comparing two nanofluids at fixed PWR, i.e., 40:60 PWR containing 5 nm and 30 nm Al_2O_3. From case (i), it was found that the 90:10 PWR of MWCNT: Al_2O_3 with 5 nm Al_2O_3 is better stable than that of 40:60 PWR containing 30 nm Al_2O_3. In case (ii), the absorbance values are higher in the nanofluids containing smaller-sized Al2O3 particles (5 nm). These could be attributed to the higher particle occupancy ratio of smaller-sized particles within a given nanofluid volume, thus ensuring more absorbance of spectral light. The result is contrary to large-sized particles signifying a lower particle occupancy ratio. In addition, if the particles within the nanofluid agglomerate resulted in instability, then the UV light absorbance would have been very low. From Fig. 9, the relatively constant absorbance values signify the excellent stability of the nanofluids. From literature [47], we learned that the wavelength of Al_2O_3/water was 225 nm, whereas in our case, the wavelength ranged between 292 and 303 nm. The variation in this wavelength must be associated with the particle hybridization at different PWR.

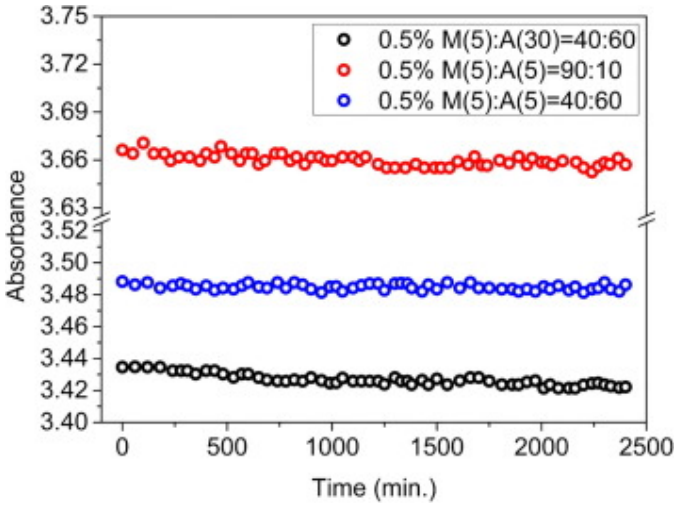

Fig. 9. Stability quantification by UV–Vis spectrophotometer.

3.5.4. Visual inspection method

Apart from confirming the even distribution of particles within the dried hybrid particles through the TEM image and the stability of the synthesized fluids by UV–Vis, viscous evaluation, and zeta potential, we did a visual inspection (Fig. 10) to rule out the possibility of particle settling. While performing the visual inspection once in 15 days, we could not see any particle settling until the end of 4 months between June and September 2021

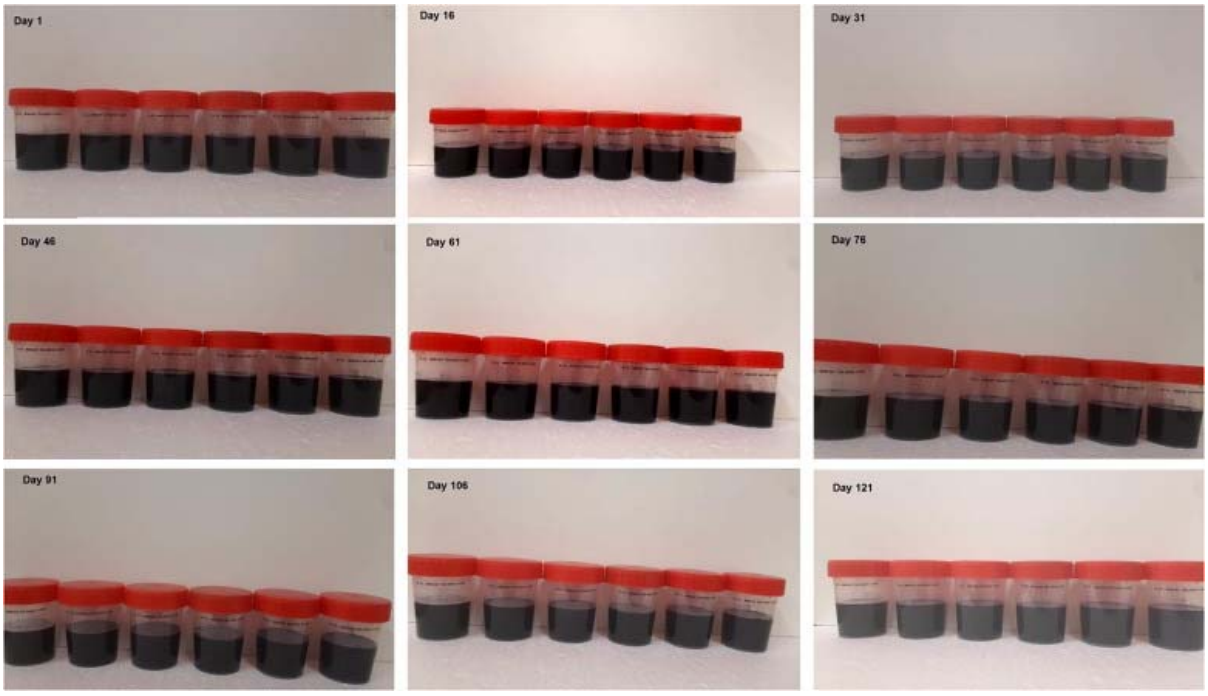

Fig. 10. Investigating the stability through visual inspection over 4 months.

3.6. Particle size effects

The particle sizes could predominantly vary the properties of the powder and thus the fluids with which it is associated, especially when the particles are of the size order of nanometres. With a thumb rule known from the existing works of literature, the small size particles possess a higher surface to volume ratio that is conclusive of their reachability as a potential thermo-enhancive material. Hence, from one of our previous works [40], we found that a blend of 5 nm MWCNT and 30 nm Al_2O_3 dispersed in DI water at a 40:60 ratio possessed enhanced chemical, physical and thermal properties when compared with other ratios. We synthesized the nanofluids with 5 nm MWCNT and 5 nm Al_2O_3 by a similar method and measured the pH, electrical conductivity, viscosity, and thermal conductivity at 0.1% concentration for PWR of 80:20, 60:40, 40:60, and 20:80. The difference in particle sizing is for the change in the size of alumina (5 nm and 30 nm) with the size of MWCNT unchanged.

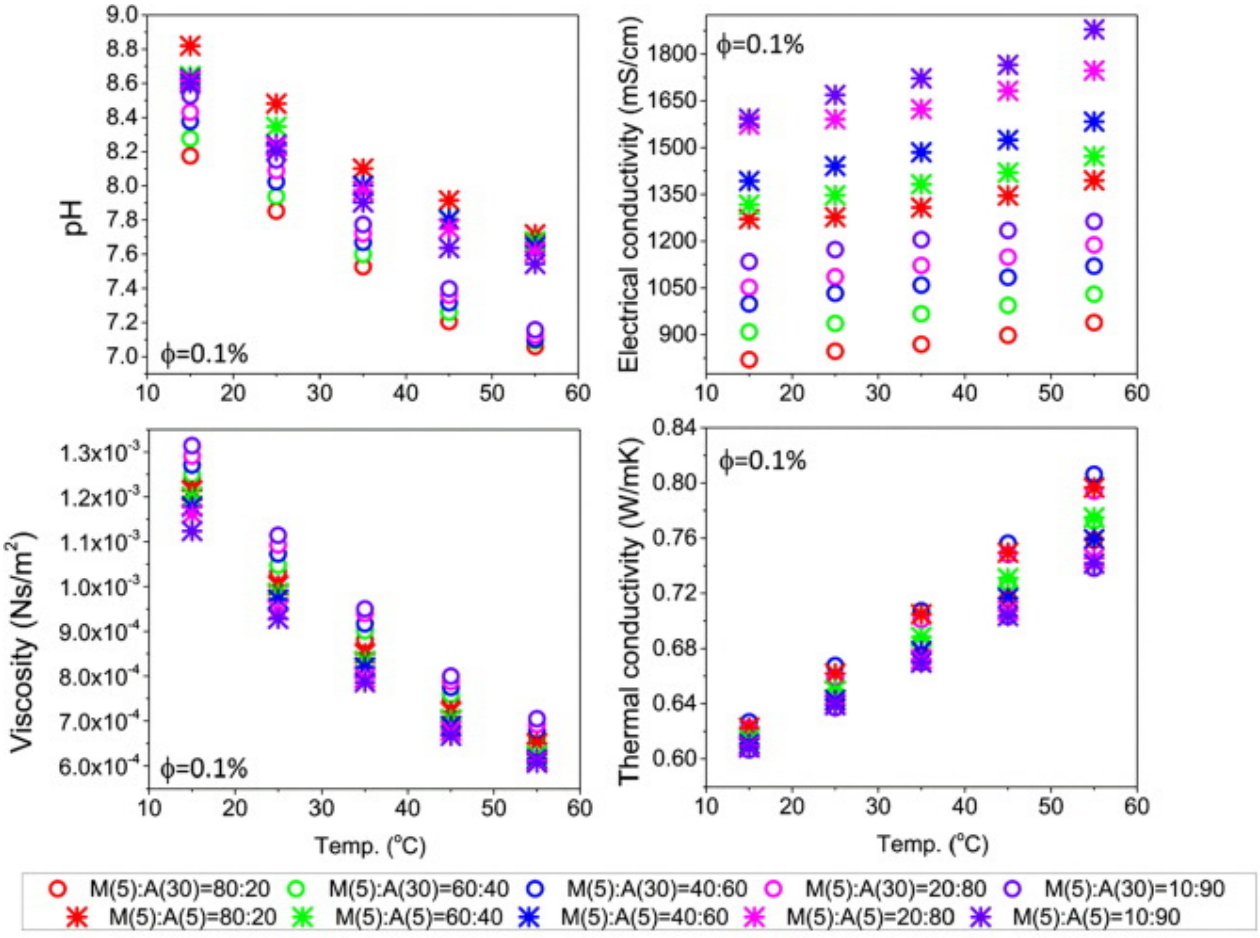

Fig. 11. Effect of particle size on φ = 0.1% nanofluid properties synthesised with powders mixed under varied particle weight ratio.

3.6.1. Chemico-physical study

The evaluation of the chemico-physical nature of nanofluids could be by measuring the acidic or basicity nature of the nanofluids. Measuring the pH of these nanofluids serves such a purpose. From Fig. 11, it was lucidly evident that all the nanofluids possessed higher pH than water, which might be due to the dispersed nanopowders getting associated or dissociated with H^+ and OH^- ions due to the base fluid-surfactant-particle interaction mechanism as discussed in Section 3.3.

It was evident that the pH decreases with increasing temperature as the NaOH formed during the base fluid-surfactant-particle interaction. At higher temperatures, NaOH could have dissociated into Na^+ and OH^- ions wherein the former would have associated with the tail of surfactant and the latter would have neutralized while associating with the free H^+ ions on the alumina particles, thus reducing the basicity and reaching the neutrality as that of water. It was also observable from Fig. 11 that the highest pH at a specific temperature in the case of 30 nm-sized alumina corresponds to 10:90, whereas in the case of 5 nm-sized alumina, it corresponded to an 80:20 ratio. The contrasting reason could be associated with the particle size involved in the dissociation of H^+ and OH^- ions during the micelle formation, apart from the interaction of surfactant with base fluid and powder surfaces.

It was evident from the works of Konakanchi et al. [48] that the ones with a larger particle size have high pH. In the case of fluid containing the 10:90 ratio, alumina possesses a larger particle size, and hence it aided in dissociation of H^+ and OH^- ions similar to the 80:20 ratio of nanofluids containing comparatively larger sized MWCNT than 5 nm alumina. However, when pH is compared based on particle size, fluid containing 5 nm alumina has more pH than fluid containing 30 nm-sized particles. The reason is nowhere different from the one stated earlier. The more the MWCNT means that the hydrophobic nature of carbon nanotubes makes us add more surfactant that produces more NaOH that on dissociation creates more OH^- ions causing high basicity compared to those with fluids containing larger sized alumina or relatively smaller sized MWCNTs.

3.6.2. Electro-physical study

Despite the diversified significance of electrical conductivity characteristics of nanofluids, ignorance of them in most of the existing studies is evident from the available pieces of literature. Amidst many studies to evaluate nanofluid stability, the electrical conductivity might provide more light on the dispersibility of the particles within the nanofluids. The electrical conductivity studies were performed on the nanofluids with different PWR for two different sizes of Al_2O_3 (30 nm and 5 nm) mixed with common-sized MWCNT (5 nm) at 0.1% volume concentrations. It is indicative from Fig. 11 that the electrical conductivity of the 10:90 ratio nanofluids was higher in both the cases containing either 30 nm alumina or 5 nm alumina. While comparing the electrical conductivity based on particle size, 30 nm alumina-based nanofluids result in a lower value than 5 nm alumina-based nanofluids. It must be due to the effective particle charge density of the particles that tend to enhance when their size gets reduced. Besides, based on the mechanism explained in section 3.4, alumina stands as a binding mediator between the water, surfactant, and MWCNT. The alumina that associates promptly with water also associates with the surfactant with the hydrophobic

tail. While one oxygen bond in the alumina breaks to associate with MWCNT, the NaOH formed due to interaction between water and SDS gets dissociated as Na^+ counter ions. These ions might increase with an increased fluid temperature, thus initiating an association with the hydrophobic tails as smaller micelles, thus raising the electrical conductivity. So lesser particle size means more particles would be available, besides having more surface charge on each particle. In the case of higher PWR, where MWCNT concentration is high, these counter ions do not have the required tails to get associated thence form NaOH when reacting with dissociated OH^- thus reducing pH. These might have resulted in the opposite behavior of pH to electrical conductivity while prone to varying temperatures.

3.6.3. Thermo-physical studies

3.6.3.1. Viscosity

In general, when the size of the particle is lesser, it means a more surface-to-volume ratio that enhances the viscosity of the nanofluids. But in our case, we noted a contradictory behavior, wherein the fluid with a larger sized particle causes additional viscous behavior than the one with smaller particle size. Similar nature of contradictory inferences has also been reported earlier [49]. If the particles are all spherical and the fluid contains only such shaped particles, they would have rolled around each other during the kinetic movement within the fluids. If the fluid is prone to one spherical particle and another tubular particle, the surface contact between such particles causes enhanced viscosity. As notable from Fig. 11, it is understood that the nanofluids dealing with a large-sized Al_2O_3 (30 nm) seem to impinge more flow resistance than the ones with small-sized Al_2O_3 (5 nm). It could be attributed to the excess surface contact points between large-sized alumina and MWCNTs, whereas it is lower surface interaction in the case of smaller particles. However, the large-sized alumina tends to acquire more surfactant molecules on their surface and can bind MWCNTs which might form slightly larger aggregates that could have also been contributing to higher viscous behavior. These aggregates might also be due to the smaller EDL, indicative of the lower electrical conductivity of the fluids with smaller-sized Al_2O_3 (5 nm). When we compared the viscosities regarding similar PWR, we observed that the fluids behaved in a contrasting nature, or in other words, the viscosities in the order of higher to lower values can be 10:90, 20:80, 40:60, 60:40, 80:20 in case of fluids with 5 nm MWCNT and 30 nm Al_2O_3, whereas it is aptly the mirrored way in case of samples with 5 nm MWCNT and 5 nm Al_2O_3. The most relevant reason could be the encapsulation of tiny hydrophobic MWCNT around the large-sized alumina that needs more surfactant for stability, causing flow resistances. In the other case, small-sized alumina seems to be evenly distributed around the MWCNTs, whereas the hydrophilic alumina supports the low use of surfactant for better dispersion, thus reducing the viscous behavior within the fluids.

3.6.3.2. Thermal conductivity

As discussed before, the reduced particle size possesses a more surface-area-to-volume ratio that provides space for more charged ions to be associated with the surface. However, this concept applies to a case where the fluid has one particle involved in the action. When there are two particles dispersed inside the base fluid, apart from the particle size playing a role in the properties, the way they bond to each other and the number of charges it carries

apart from the pH of the base fluid play significant roles. So there must be an optimal balance between their influential natures to enhance the thermal conductivity of nanofluids. From Fig. 11, it is observable that the 40:60 ratio nanofluid containing 30 nm Al_2O_3 possesses higher thermal conductivity than the rest of its group of nanofluids, whereas the 80:20 ratio nanofluid with 5 nm Al_2O_3 fared the best amidst its group of nanofluids with similar particle size. It could be attributed to the equiproportional contribution of the nanopowders through their unique thermal conductivity values in combination with their particle sizes. Besides, the surfactant being a base can slightly deteriorate the properties if excess MWCNT is in the case of dispersion. However, in the case of fluid containing 5 nm-sized particles, the particle size effects might have dominated more apart from the thermal conductivity of the individual powders.

To conclude, Table 2 shows the enhancement in the properties of nanofluids based on the particle size and particle weight ratio at 0.1% concentration.

Table 2. Property enhancement of 0.1% Conc. different sized particle based nanofluid over DI water.

M:A size (nm)	Fluid PWR	pH Enhan. %		σ Enhan. %		μ Enhan. %		k Enhan. %	
		High	Low	High	Low	High	Low	High	Low
5:30	80:20	7.4	0.4	64.4	52.1	15.0	10.5	18.5	4.2
5:30	60:40	8.7	0.9	80.4	68.6	15.7	11.5	20.7	4.8
5:30	40:60	10.1	1.0	96.1	85.3	17.7	13.2	**25.9**	**7.3**
5:30	20:80	10.8	1.4	108.1	95.2	19.5	15.3	24.0	6.5
5:30	10:90	**12.0**	**1.8**	**121.2**	**110.4**	**21.7**	**17.5**	15.3	3.8
5:5	80:20	**15.9**	**9.8**	144.3	135.8	**12.0**	**8.4**	**24.4**	**6.6**
5:5	60:40	13.6	9.2	157.8	144.4	11.1	3.9	21.1	5.1
5:5	40:60	13.3	8.7	177.3	158.5	9.1	2.5	18.6	4.6
5:5	20:80	13.2	8.3	206.0	192.0	7.6	1.8	16.4	4.3
5:5	10:90	13.0	7.3	**229.1**	**195.5**	4.0	1.1	15.9	4.1

3.7. Properties at a different particle weight ratio

Now it is apparent the fluctuating properties of the nanofluids through the dispersion of different sized particles experiments were carried out by testing the capabilities of the hybrid nanofluids with a 90:10 ratio involving 5 nm Al_2O_3. We performed them as we knew that the PWR 40:60 containing 30 nm Al_2O_3 and the 80:20 ratio with 5 nm Al_2O_3 fared the best in almost all properties.

3.7.1. pH

It was, as usual, to find from Fig. 12 that the pH of the nanofluids reduced with increment in fluid temperature for the reasons stated in previous sections. Besides, the PWR 90:10 had higher pH than the rest of it. Therefore, the nanofluids with pure MWCNTs had a pH higher than those fluids with Al_2O_3, which is the logic behind the high value of pH in the case of nanofluids containing a higher ratio MWCNTs. The excess MWCNTs tend for excess surfactant that reacts with water to form more NaOH, leading to dissociation of OH^- ions during lower temperatures. These OH^- ions convert the fluid to basicity conditions, thus making its pH higher. However, the rise in fluid temperature enhances the kinetic energies of the molecules that excited the molecular vibrations leading to the dissociation of water molecules, thus leading to more H^+ ions causing a decreased pH.

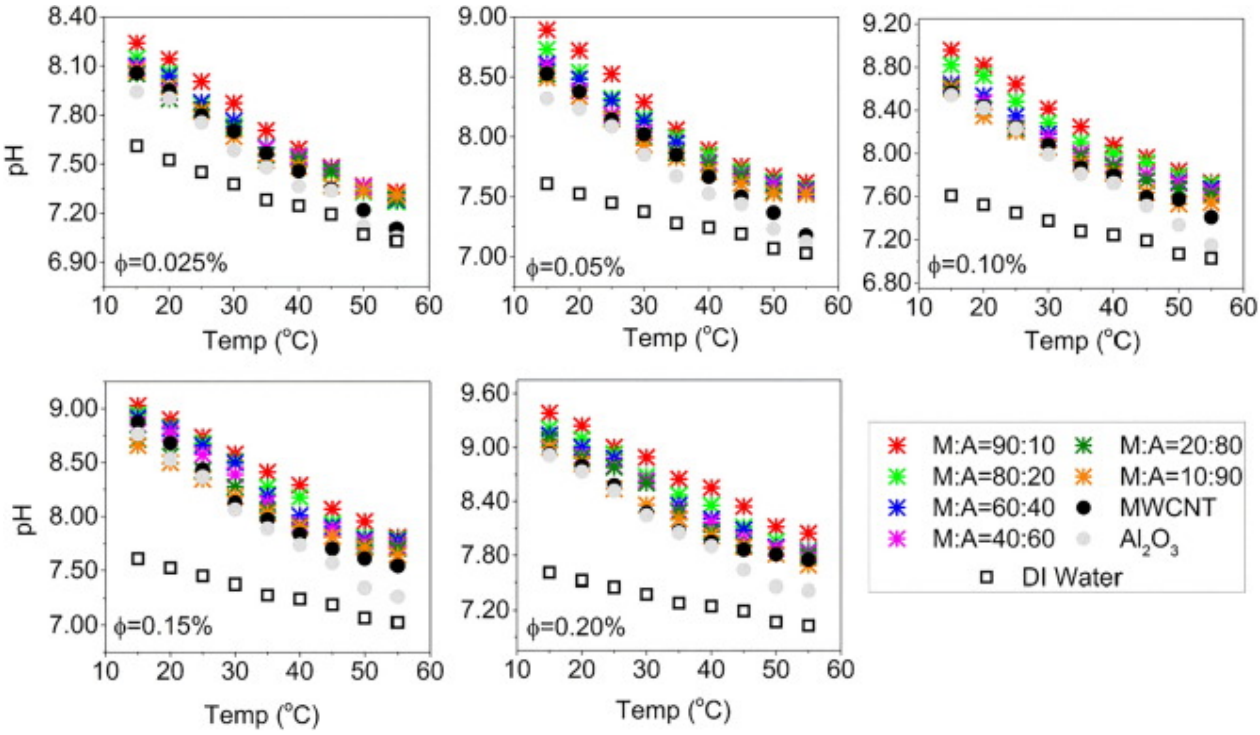

Fig. 12. Influence of varied temperature and volume concentration on the pH of different PWR based nanofluids.

3.7.2. Electrical conductivity

We measured the electrical conductivity of the fluid samples at different temperatures under varied volume concentrations. It is observable from Fig. 13 that the electrical conductivity enhanced up to 0.2% concentration and began plateauing up to 0.5%. The maximum value was for pure Al_2O_3 at 0.2% for 55 °C, as the electrical conductivity of Al_2O_3 is higher than that of MWCNT. Hence, it is unmistakable that the hybridization of these particles would result in conductivity lesser than Al_2O_3. Based on different PWR, under similar concentration and temperature conditions, we inferred the maximum value at PWR 10:90.

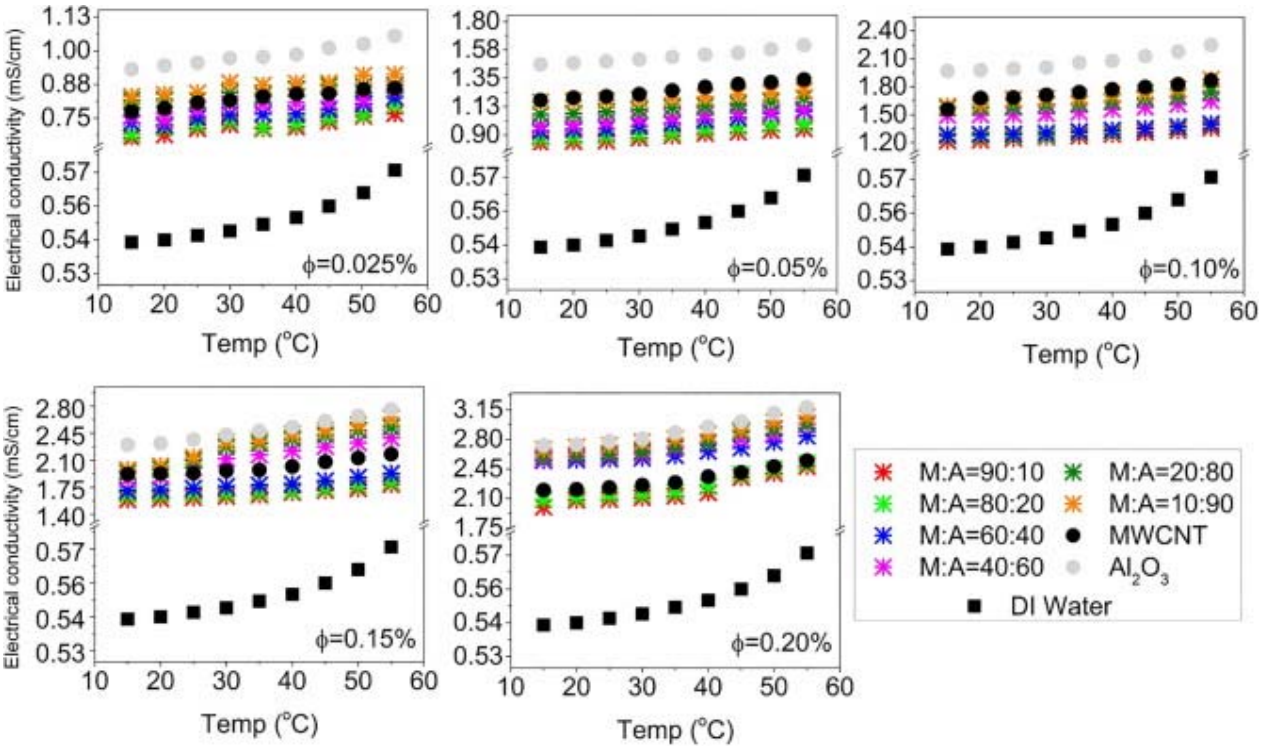

Fig. 13. Influence of varied temperature and volume concentration on the Electrical Conductivty of different PWR based nanofluids.

Besides, the electrical conductivity began to lower from 60 °C for all classes of fluids. Therefore, the enhanced electrical conductivity of the nanofluids compared to the base fluid must be due to the net charges around the particle, and thus the formation of an Electrical Double Layer (EDL).

The reason for contrasting results beyond 0.2% and 55 °C is because the electrical conductivity has a complex dependence on the pH, ionic and volume concentrations, and EDL. In specific, when the dispersion of alumina happens within polar fluids such as DI water, electric charge forms around the particle surfaces. Counter ions are attracted towards these charges to form a diffuse layer or the electrical double layer signified by Debye length [50]. The matter of concern in our experiments is that the net electric charge density might be higher on the interactive surfaces due to low ionic strength resulting in insufficient ionic concentration for electric charge compensation. Thus the combined ionic concentration and charge over the particle surface that forms the EDL is the reason for enhanced electrical conductivity due to electrophoretic mobility within the nanodispersion. It might also be why at higher temperatures, electrophoretic mobility and thermophoretic mobility causes a decrease in pH and an increase in the electrical conductivity to a limit of particle dispersion and temperature. Besides, furthermore generation of conducting pathways at increased volume concentration attenuates the electrical conductivity. However, when the volume concentration crosses 0.2% and is at 0.5%, the number of particles added is so much that the EDL formation is insufficient, thus leading to the intense electrostatic attraction between particles in the nanofluids. These are the reasons for the

halt in experiments beyond 0.2% concentration on measuring pH and electrical conductivity of nanofluids.

3.7.3. Viscosity

Significantly, the dispersion of two different nanopowders with general characteristics of either being -phobic or -philic with water molecules can augment or detriment the viscous behavior of the fluid on the whole. From Fig. 14, it is observable that the addition of two different nanoparticles at diverse PWRs into the base fluid augmented the viscous behavior of that fluid. Though it might imply the dense nature of the nanoparticles and nanotubes, they must also be visualized based on their nature while interacting with the water molecules. For example, while alumina readily reacts with water, MWCNT behaves opposite exactly, forcing an additional reaction of surfactant molecules with MWCNT to ensure a stable nanofluid. Thus, the addition of MWCNT means higher PWR, possessing high viscosity.

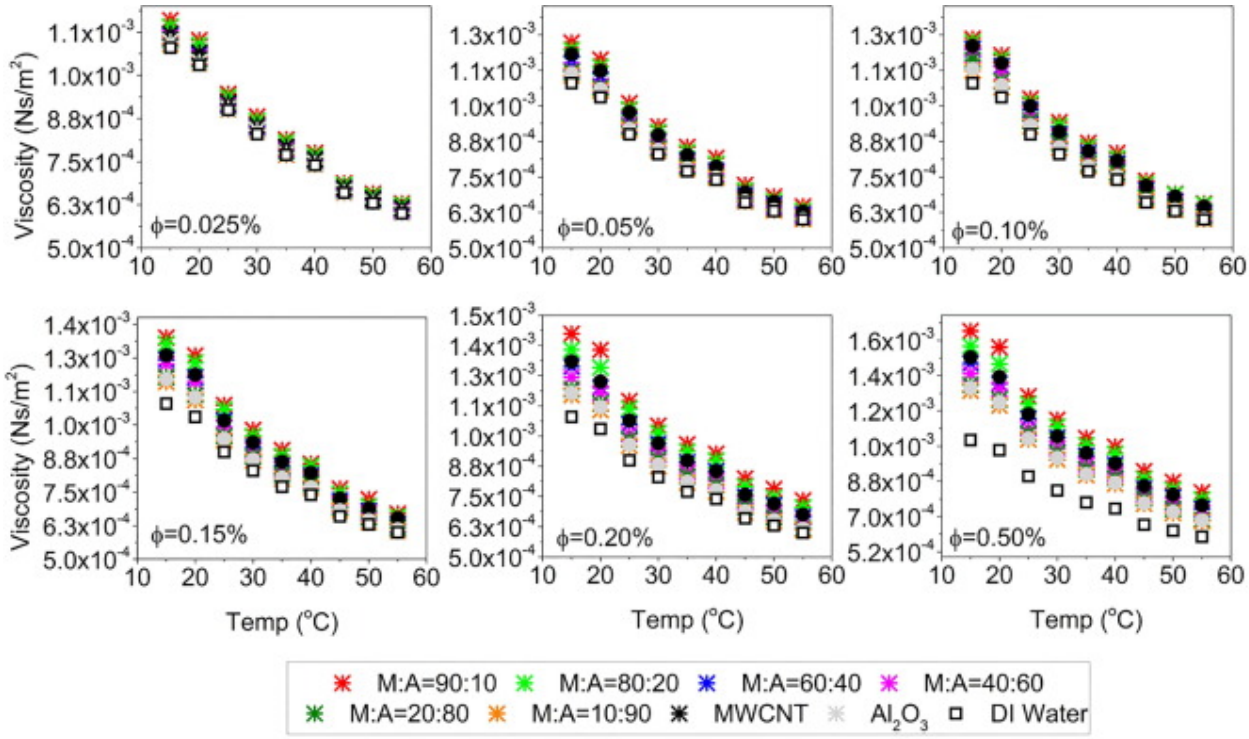

Fig. 14. Influence of varied temperature and volume concentration on the viscosity of different PWR based nanofluids.

Besides, the availability of two different particles of two different shapes can have an interaction mechanism and bonding nature that influences the viscous behavior of the fluid with which it is associated. Such mechanisms support intense intermolecular force between the particles themselves and between particle and fluid molecules, thus reducing the Brownian kinetics, and hence the fluid resistance prevails. But such resistances are overcome by a higher temperature that promotes Brownian interaction, thus weakening such intermolecular forces leading to detrimental viscous behavior.

3.7.4. Thermal conductivity

The thermal conductivity of the nanofluids enhances with an increase in particle loading and temperature. Enhancement due to particle loading is much more significant than the temperature effects. The encapsulation of the liquid molecules around the particle surface, thus forming a thermal bonding between the particle and fluid molecules, is the cause of enhanced thermal conductivity and energy transport. The energy transport is due to micro convection effects within the fluid generated by the Brownian motion of the particles. The increase in temperature generates Brownian convection, and excess particles within it promote random movement of particles causing enhanced thermal conductive behaviour.

In case of variations regarding PWR, the 90:10 ratio fares best at all volume concentrations, as observable from Fig. 15. MWCNTs are hydrophobic in nature and are less dense, which tends to lower particle Reynolds number, which does not enhance the thermal conductivity multifold though it has a value of 2000 W/mK. Hence, the rise in thermal conductivity for the 90:10 ratio must be attributed to the higher thermal properties of MWCNT instead of the dense alumina that bonds with surfactant and binds the MWCNTs around it. So the effect of the Brownian motion must be dominative due to the denser particle that causes the movement of MWCNTs around the fluid molecules that promote excess thermal conductivity.

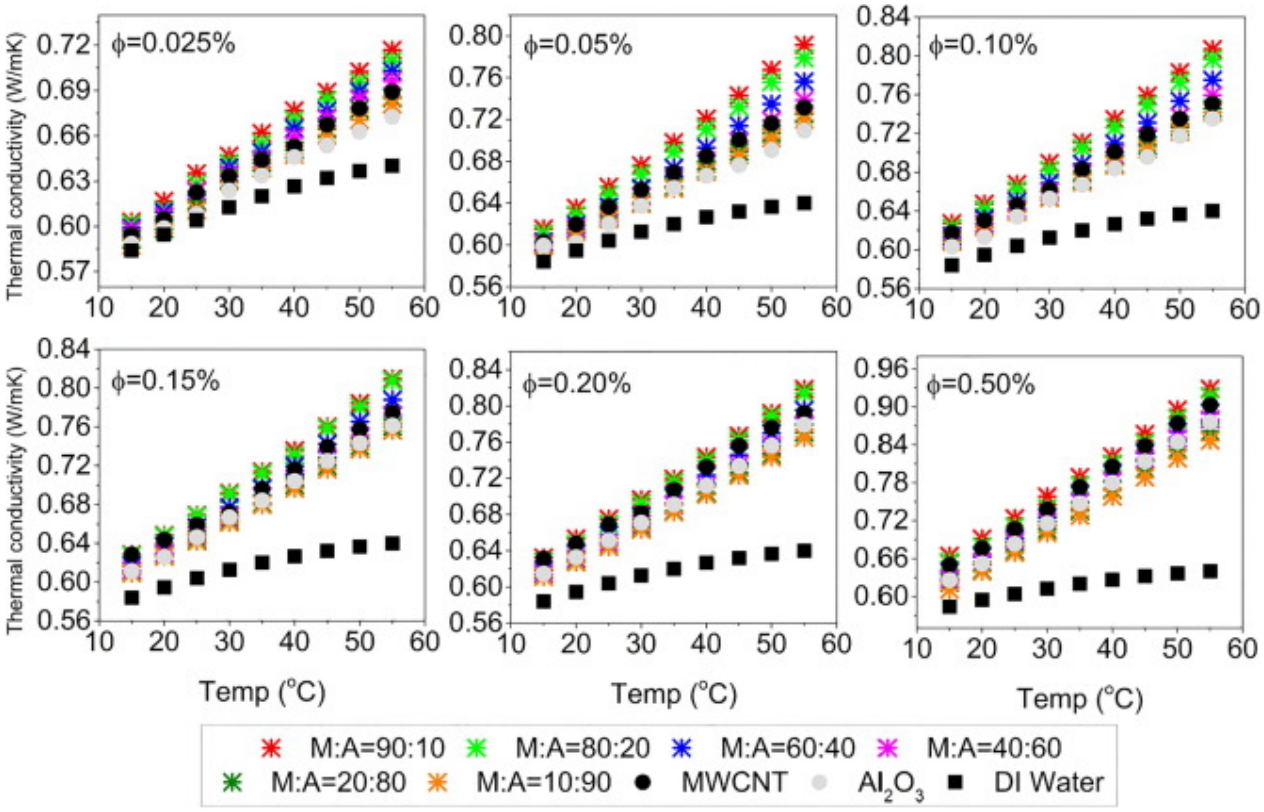

Fig. 15. Influence of varied temperature and volume concentration on the Thermal Conductivity of different PWR based nanofluids.

Hence, it is conclusive from the results that the surface charges must be significantly available to ensure electrostatic repulsion between particles for better stability and for Brownian convection to enhance the thermal properties of the nanofluids. To conclude, Table 3 displays the enhancement in the properties of nanofluids based on the volume concentration and particle weight ratio.

Table 3. Property enhancement of 90:10 PWR nanofluid over DI water.

ϕ	pH Enhan. %		σ Enhan. %		μ Enhan. %		k Enhan. %	
	Highest	Lowest	Highest	Lowest	Highest	Lowest	Highest	Lowest
0.025%	8.3	4.3	34.3	28.8	7.4	4.9	12.0	3.3
0.05%	16.8	8.4	66.4	55.3	13.3	7.8	23.7	5.4
0.10%	17.7	10.0	138.2	126.5	14.5	9.5	26.0	7.4
0.15%	18.6	11.1	213.0	195.0	22.7	11.7	26.5	7.6
0.20%	**23.3**	**14.5**	**248.3**	**238.2**	31.8	22.3	27.9	8.3
0.50%	–	–	–	–	**57.3**	**40.9**	**45.1**	**13.7**

3.8. Correlation development

As the existing correlations suggested by Giwa et al. [40] did not suit the measurement of pH, EC, and viscosity, new correlations were evolved based on the measured data. Besides, the correlation for thermal conductivity is also generated based on the PWR, volume concentration, and temperature. Before suggesting the suitability of correlations, the PWR is to be read as 0.9, 0.8, 0.6, 0.4, 0.6, 0.2, and 0.1 for 90:10, 80:20, 60:40, 40:60, 20:80, and 10:90 respectively. The correlations predicted for pH and viscosity are applicable for the volume concentration between 0.025 and 0.2%, temperature between 15 and 55 °C, and PWR between 0.1 and 0.9. However, the viscosity and thermal conductivity correlations are extendable to 0.5% as per the conditions stated above. The viscosity and thermal conductivity correlations are also applicable to mono-particle nanofluids in above-stated scenario. The general way of expressing the correlation is as follows.

Table 4 lists the constants A_1 to A_{11}, whereas Table 5 details the deviation limit between the correlated and experimental values, R^2, and standard error values.

Table 4. Constants for the generalized correlation.

Parameter	A_1	A_2	A_3	A_4	A_5	A_6	A_7	A_8	A_9	A_{10}	A_{11}
Relative pH	1.0245	4.15 x10^{-3}	0.7564	−9.46 x10^{-3}	3.098 x10^{-2}	7.222 x10^{-2}	−1.15 x10^{-3}	3.893 x10^{-3}	−1.7 x10^{-4}	1.95 x10^{-6}	3.076 x10^{-2}
Relative Electrical conductivity	1.2288	−5.2 x10^{-4}	19.429	0.1313	−1.0415	0.6322	8.059 x10^{-3}	−0.1517	−5.2 x10^{-5}	−32.492	0.3796
Relative Viscosity	0.9931	−6.5 x10^{-4}	0.6335	−4.3 x10^{-3}	0.1134	0.3361	−5.1 x10^{-4}	4.6 x10^{-6}	2.12 x10^{-6}	−0.2234	3.006 x10^{-2}
Relative thermal conductivity	1.0111	−1.39 x10^{-3}	0.1452	1.153 x10^{-2}	2.842 x10^{-2}	0.1166	1.14 x10^{-3}	−1.15 x10^{-3}	4.29 x10^{-5}	−0.451	−2.63 x10^{-2}

Table 5. Deviation limit, R square and Standard error values for the predicted correlation.

Correlation for	Deviation from experimental data	R square	Standard error
Relative pH	−3.46 to 3.05%	0.9160	0.0133
Relative Electrical conductivity	−9.42 to 5.88%	0.9926	0.0856
Relative Viscosity	−9.35 to 4.64%	0.9394	0.0255
Relative thermal conductivity	−5.74 to 6.83%	0.9535	0.0184

4. Conclusion

Based on the optimized Dispersion Fraction, sonicating time and sonication amplitude, the nanofluids were prepared at different PWR using MWCNT and Al_2O_3 by a stabilizing agent, SDS. The experiments were carried out to predict the effect of Al_2O_3 particle size on the nanofluid properties to identify the best PWR based on particle sizes. The conclusion could be derived as follows:

a. The XRD, SEM and DLS results confirm the average crystallite size, particle size and hydrodynamic size of the particles to be < 5 nm, 15 nm, and 39 nm.
b. The hydrodynamic bonding between the particles that signifies the uniform distribution of the dispersed constituents is evident from the TEM image.
c. The nanofluid stability is much appreciable based on the zeta potential measurement, transient viscous data, and UV–Vis studies apart from the visual inspection made for four months.
d. Maximum enhancement of pH, electrical conductivity and viscosity by 12%, 121% and 22%, respectively, were noted in the 10:90 MWCNT: Al_2O_3 nanofluids with 30 nm Al_2O_3 and thermal conductivity enhancement by 26% at 40:60 MWCNT: Al_2O_3.
e. Maximum enhancement of pH, viscosity and thermal conductivity by 16%, 12% and 24%, respectively, in 90:10 MWCNT: Al_2O_3 nanofluids with 5 nm Al_2O_3 and electrical conductivity enhancement by 229% at 10:90 MWCNT: Al_2O_3.
f. Based on positive property requisites of a nanofluid, the best PWR is 40:60 MWCNT: Al_2O_3 with 30 nm Al_2O_3 and the 90:10 MWCNT: Al_2O_3 with 5 nm Al_2O_3.
g. The correlations for all the properties were developed as a function of temperature, volume concentration, and PWR, with the maximum deviation between the correlated and experimental data to be less than ± 10%, which is generally a good agreement.

Funding

This research did not receive any specific grant from funding agencies in the public, commercial, or not-for-profit sectors.

CRediT authorship contribution statement

S. Suseel Jai Krishnan: Validation, Formal analysis, Investigation, Writing – original draft. **M. Momin:** Data curation, Writing – original draft. **C. Nwaokocha:** Writing – original draft,

Visualization. **M. Sharifpur:** Methodology, Writing – review & editing, Supervision. **J.P. Meyer:** Resources, Project administration.

Declaration of Competing Interest

The authors declare that they have no known competing financial interests or personal relationships that could have appeared to influence the work reported in this paper.

References

1. M. Sharifpur, S.O. Giwa, K.-Y. Lee, H. Ghodsinezhad, J.P. Meyer, Experimental investigation into natural convection of zinc oxide/water nanofluids in a square cavity, Heat Transfer Eng. 42 (2021) 1675–1687, https://doi.org/10.1080/01457632.2020.1818384.
2. Z. Said, M. Jamei, L. Syam Sundar, A.K. Pandey, A. Allouhi, C. Li, Thermophysical properties of water, water and ethylene glycol mixture-based nanodiamond +Fe_3O_4 hybrid nanofluids: an experimental assessment and application of data-driven approaches, J. Mol. Liquids 347 (2022), https://doi.org/10.1016/j.molliq.2021.117944.
3. S.J.K. Sasidharan, N. Parasumanna Krishnamurthy, R. Mamat, V.D. Loganathan, R. Sathyamurthy, Synthesis, characterisation and thermo-physical investigations on magnesia nanoparticles dispersed in ethylene glycol–DI water (50:50), Micro Nano Lett. 13 (2018) 335–340, https://doi.org/10.1049/mnl.2017.0484.
4. M. Sandhya, D. Ramasamy, K. Kadirgama, W.S.W. Harun, R. Saidur, Experimental study on properties of hybrid stable & surfactant-free nanofluids GNPs/CNCs (Graphene nanoplatelets/cellulose nanocrystal) in water/ethylene glycol mixture for heat transfer application, J. Mol. Liq. 348 (2022), https://doi.org/10.1016/j.molliq.2021.118019 118019.
5. P. Selvan, D. Jebakani, K. Jeyasubramanian, D. Jones Joseph Jebaraj, Enhancement of thermal conductivity of water based individual and hybrid SiO2/Ag nanofluids with the usage of calcium carbonate nano particles as stabilizing agent, J. Mol. Liquids 345 (2022), https://doi.org/10.1016/j.molliq.2021.117846.
6. M.E. Mondejar, M. Regidor, J. Krafczyk, C. Ihmels, B. Schmid, G.M. Kontogeorgis, F. Haglind, An open-access database of the thermophysical properties of nanofluids, J. Mol. Liq. 333 (2021), https://doi.org/10.1016/j.molliq.2020.115140 115140.
7. S. Suseel Jai Krishnan, P.K. Nagarajan, Influence of stability and particle shape effects for an entropy generation based optimized selection of magnesia nanofluid for convective heat flow applications, Appl. Surf. Sci. 489 (2019) 560–575, https://doi.org/10.1016/j.apsusc.2019.06.038.
8. R. Lenin, P.A. Joy, C. Bera, A review of the recent progress on thermal conductivity of nanofluid, J. Mol. Liq. 338 (2021), https://doi.org/10.1016/j.molliq.2021.116929 116929.
9. L. Qiu, N. Zhu, Y. Feng, E.E. Michaelides, G. Żyła, D. Jing, X. Zhang, P.M. Norris, C. N. Markides, O. Mahian, A review of recent advances in thermophysical properties at the nanoscale: From solid state to colloids, Phys. Rep. 843 (2020) 1–81, https://doi.org/10.1016/j.physrep.2019.12.001.
10. S. Ebrahimi, S.F. Saghravani, Experimental study of the thermal conductivity features of the water based Fe_3O_4/CuO nanofluid, Heat Mass Transf. 54 (2018) 999–1008, https://doi.org/10.1007/s00231-017-2188-z.

11. A.H.A. Al-Waeli, M.T. Chaichan, H.A. Kazem, K. Sopian, Evaluation and analysis of nanofluid and surfactant impact on photovoltaic-thermal systems, Case Stud. Thermal Eng. 13 (2019), https://doi.org/10.1016/j.csite.2019.100392100392.
12. R.E. Morsi, R.A. El-Salamony, Effect of cationic, anionic and non-ionic polymeric surfactants on the stability, photo-catalytic and antimicrobial activities of yttrium oxide nanofluids, J. Mol. Liq. 297 (2020), https://doi.org/10.1016/j.molliq.2019.111848 111848.
13. M.U. Sajid, H.M. Ali, Recent advances in application of nanofluids in heat transfer devices: a critical review, Renew. Sustain. Energy Rev. 103 (2019) 556–592, https://doi.org/10.1016/j.rser.2018.12.057.
14. H. Pourpasha, S. Zeinali Heris, Y. Mohammadfam, Comparison between multi-walled carbon nanotubes and titanium dioxide nanoparticles as additives on performance of turbine meter oil nano lubricant, Sci. Rep. 11 (2021) 11064, https://doi.org/10.1038/s41598-021-90625-5.
15. D.S. Adelekan, O.S. Ohunakin, M.H. Oladeinde, G. Jatinder, O.E. Atiba, M.O. Nkiko, A.A. Atayero, Performance of a domestic refrigerator in varying ambient temperatures, concentrations of TiO_2 nanolubricants and R600a refrigerant charges, Heliyon 7 (2021), https://doi.org/10.1016/j.heliyon.2021.e06156e06156.
16. W. Safiei, M.M. Rahman, A.R. Yusoff, M.N. Arifin, W. Tasnim, Effects of SiO_2-Al_2O_3-ZrO_2 Tri-hybrid nanofluids on surface roughness and cutting temperature in end milling process of aluminum alloy 6061–T6 using uncoated and coated cutting inserts with minimal quantity lubricant method, Arab. J. Sci. Eng. 46 (2021) 7699–7718, https://doi.org/10.1007/s13369-021-05533-7.
17. A.S. Sowmyashree, A. Somya, C.B.P. Kumar, S. Rao, Novel nano corrosion inhibitor, integrated zinc titanate nano particles: Synthesis, characterization, thermodynamic and electrochemical studies, Surf. Interfaces 22 (2021), https://doi.org/10.1016/j.surfin.2020.100812 100812.
18. M.M. Souby, M.H.S. Bargal, Y. Wang, Thermohydraulic performance improvement and entropy generation characteristics of a microchannel heat sink cooled with new hybrid nanofluids containing ternary/binary hybrid nanocomposites, Energy Sci. Eng. 9 (2021) 2493–2513, https://doi.org/10.1002/ese3.982.
19. M. Bahiraei, M. Jamshidmofid, M. Goodarzi, Efficacy of a hybrid nanofluid in a new microchannel heat sink equipped with both secondary channels and ribs, J. Mol. Liq. 273 (2019) 88–98, https://doi.org/10.1016/j.molliq.2018.10.003.
20. J.P. Vallejo, E. Sani, G. _Żyła, L. Lugo, Tailored silver/graphene nanoplatelet hybrid nanofluids for solar applications, J. Mol. Liq. 296 (2019), https://doi.org/10.1016/j.molliq.2019.112007 112007.
21. M.M. Bhatti, H.F. Öztop, R. Ellahi, I.E. Sarris, M.H. Doranehgard, Insight into the investigation of diamond (C) and Silica (SiO_2) nanoparticles suspended in water-based hybrid nanofluid with application in solar collector, J. Mol. Liq. 357 (2022), https://doi.org/10.1016/j.molliq.2022.119134 119134.
22. N.A.S. Muzaidi, M.A. Fikri, K.N.S. Wan Salihin Wong, A.Z. Mohammad Sofi, R. Mamat, N. Mohd Adenam, M.Y.A. Mat Yunin, H.K. Adli, Heat absorption properties of $CuO/TiO_2/SiO_2$ trihybrid nanofluids and its potential future direction towards solar thermal applications, Arab. J. Chem. 14 (2021), https://doi.org/10.1016/j.arabjc.2021.103059.
23. S. Jana, A. Salehi-Khojin, W.-H. Zhong, Enhancement of fluid thermal conductivity by the addition of single and hybrid nano-additives, Thermochim Acta 462 (2007) 45–55, https://doi.org/10.1016/j.tca.2007.06.009.
24. M. Chopkar, S. Kumar, D.R. Bhandari, P.K. Das, I. Manna, Development and characterization of Al2Cu and Ag2Al nanoparticle dispersed water and ethylene glycol based nanofluid, Mater. Sci. Eng., B 139 (2007) 141–148, https://doi.org/10.1016/j.mseb.2007.01.048.
25. N. Jha, S. Ramaprabhu, Synthesis and Thermal Conductivity of Copper Nanoparticle Decorated Multiwalled Carbon Nanotubes Based Nanofluids, J. Phys. Chem. C 112 (2008) 9315–9319, https://doi.org/10.1021/jp8017309.
26. L. Chen, W. Yu, H. Xie, Enhanced thermal conductivity of nanofluids containing Ag/MWNT composites, Powder Technol. 231 (2012) 18–20, https://doi.org/10.1016/j.powtec.2012.07.028.

27. S. Askari, H. Koolivand, M. Pourkhalil, R. Lotfi, A. Rashidi, Investigation of TiO_2/Graphene nanohybrid heat transfer properties: Experimental approach, Int. Commun. Heat Mass Transfer 87 (2017) 30–39, https://doi.org/10.1016/j.icheatmasstransfer.2017.06.012.
28. N.N. Esfahani, D. Toghraie, M. Afrand, A new correlation for predicting the thermal conductivity of ZnO–Ag (50%–50%)/water hybrid nanofluid: an experimental study, Powder Technol. 323 (2018) 367–373, https://doi.org/10.1016/j.powtec.2017.10.025.
29. D. Toghraie, V.A. Chaharsoghi, M. Afrand, Measurement of thermal conductivity of ZnO–TiO_2/EG hybrid nanofluid, J. Therm. Anal. Calorim. 125 (2016) 527–535, https://doi.org/10.1007/s10973-016-5436-4.
30. S. Suresh, K.P. Venkitaraj, P. Selvakumar, M. Chandrasekar, Synthesis of Al_2O_3–Cu/water hybrid nanofluids using two step method and its thermo physical properties, Colloids Surf., A 388 (2011) 41–48, https://doi.org/10.1016/j.colsurfa.2011.08.005.
31. S. Rostami, A.A. Nadooshan, A. Raisi, An experimental study on the thermal conductivity of new antifreeze containing copper oxide and graphene oxide nano-additives, Powder Technol. 345 (2019) 658–667, https://doi.org/10.1016/j.powtec.2019.01.055.
32. Z. Aparna, M. Michael, S.K. Pabi, S. Ghosh, Thermal conductivity of aqueous Al_2O_3/Ag hybrid nanofluid at different temperatures and volume concentrations: An experimental investigation and development of new correlation function, Powder Technol. 343 (2019) 714–722, https://doi.org/10.1016/j.powtec.2018.11.096.
33. O. Soltani, M. Akbari, Effects of temperature and particles concentration on the dynamic viscosity of MgO-MWCNT/ethylene glycol hybrid nanofluid: Experimental study, Physica E 84 (2016) 564–570, https://doi.org/10.1016/j.physe.2016.06.015.
34. M. Asadi, A. Asadi, Dynamic viscosity of MWCNT/ZnO–engine oil hybrid nanofluid: An experimental investigation and new correlation in different temperatures and solid concentrations, Int. Commun. Heat Mass Transfer 76 (2016) 41–45, https://doi.org/10.1016/j.icheatmasstransfer.2016.05.019.
35. K. Motahari, M. Abdollahi Moghaddam, M. Moradian, Experimental investigation and development of new correlation for influences of temperature and concentration on dynamic viscosity of MWCNT- SiO_2 (20–80)/20W50 hybrid nano-lubricant, Chin. J. Chem. Eng. 26 (2018) 152–158, https://doi.org/10.1016/j.cjche.2017.06.011.
36. M. Hemmat Esfe, A.A. Abbasian Arani, M. Rezaie, W.-M. Yan, A. Karimipour, Experimental determination of thermal conductivity and dynamic viscosity of Ag–MgO/water hybrid nanofluid, Int. Commun. Heat Mass Transfer 66 (2015) 189–195, https://doi.org/10.1016/j.icheatmasstransfer.2015.06.003.
37. S.K. Mechiri, V. Vasu, A. Venu Gopal, Investigation of thermal conductivity and rheological properties of vegetable oil based hybrid nanofluids containing Cu–Zn hybrid nanoparticles, Experimental Heat Transfer 30 (2017) 205–217, https://doi.org/10.1080/08916152.2016.1233147.
38. K.A. Hamid, W.H. Azmi, M.F. Nabil, R. Mamat, K.V. Sharma, Experimental investigation of thermal conductivity and dynamic viscosity on nanoparticle mixture ratios of TiO_2- SiO_2 nanofluids, Int. J. Heat Mass Transf. 116 (2018) 1143–1152, https://doi.org/10.1016/j.ijheatmasstransfer.2017.09.087.
39. E.I. Chereches, A.A. Minea, Electrical conductivity of new nanoparticle enhanced fluids: an experimental study, Nanomaterials (Basel, Switzerland) 9 (2019) 1228, https://doi.org/10.3390/nano9091228.
40. S.O. Giwa, M. Sharifpur, J.P. Meyer, S. Wongwises, O. Mahian, Experimental measurement of viscosity and electrical conductivity of water-based c- Al_2O_3/MWCNT hybrid nanofluids with various particle mass ratios, J. Therm. Anal. Calorim. 143 (2021) 1037–1050, https://doi.org/10.1007/s10973-020-10041-1.
41. S.O. Giwa, M. Sharifpur, M. Goodarzi, H. Alsulami, J.P. Meyer, Influence of base fluid, temperature, and concentration on the thermophysical properties of hybrid nanofluids of

alumina–ferrofluid: experimental data, modeling through enhanced ANN, ANFIS, and curve fitting, J. Therm. Anal. Calorim. 143 (2021) 4149–4167, https://doi.org/10.1007/s10973-020-09372-w.
42. V.V. Wanatasanapan, M.Z. Abdullah, P. Gunnasegaran, Effect of TiO_2- Al_2O_3 nanoparticle mixing ratio on the thermal conductivity, rheological properties, and dynamic viscosity of water-based hybrid nanofluid, J. Mater. Res. Technol. 9 (2020) 13781–13792, https://doi.org/10.1016/j.jmrt.2020.09.127.
43. S.O. Giwa, M. Momin, C.N. Nwaokocha, M. Sharifpur, J.P. Meyer, Influence of nanoparticles size, per cent mass ratio, and temperature on the thermal properties of water-based MgO–ZnO nanofluid: an experimental approach, J. Therm. Anal. Calorim. 143 (2021) 1063–1079, https://doi.org/10.1007/s10973-020-09870-x.
44. S. Akilu, A.T. Baheta, M.A.M. Said, A.A. Minea, K.V. Sharma, Properties of glycerol and ethylene glycol mixture based SiO_2-CuO/C hybrid nanofluid for enhanced solar energy transport, Sol. Energy Mater. Sol. Cells 179 (2018) 118–128, https://doi.org/10.1016/j.solmat.2017.10.027.
45. S. Kannaiyan, C. Boobalan, A. Umasankaran, A. Ravirajan, S. Sathyan, T. Thomas, Comparison of experimental and calculated thermophysical properties of alumina/cupric oxide hybrid nanofluids, J. Mol. Liq. 244 (2017) 469–477, https://doi.org/10.1016/j.molliq.2017.09.035.
46. A. Einstein, Über die von der molekularkinetischen Theorie der Wärme geforderte Bewegung von in ruhenden Flüssigkeiten suspendierten Teilchen, Ann. Phys. 322 (1905) 549–560, https://doi.org/10.1002/andp.19053220806.
47. H. Ghodsinezhad, M. Sharifpur, J.P. Meyer, Experimental investigation on cavity flow natural convection of Al_2O_3–water nanofluids, Int. Commun. Heat Mass Transfer 76 (2016) 316–324, https://doi.org/10.1016/j.icheatmasstransfer.2016.06.005.
48. H. Konakanchi, R.S. Vajjha, G.A. Chukwu, D.K. Das, Measurements of pH of Three Nanofluids and Development of New Correlations, Heat Transfer Eng. 36 (2015) 81–90, https://doi.org/10.1080/01457632.2014.906286.
49. J.P. Meyer, S.A. Adio, M. Sharifpur, P.N. Nwosu, The viscosity of nanofluids: a review of the theoretical, empirical, and numerical models, Heat Transfer Eng. 37 (2016) 387–421, https://doi.org/10.1080/01457632.2015.1057447.
50. R.J. Hunter, Zeta potential in colloid science: principles and applications, Academic press, 2013.